Photocatalytic hydrogen production from biomass under solar irradiation

Dissertation submitted in partial fulfilment of the requirements for the award of degree of

MASTER OF SCIENCE

in

CHEMISTRY

Submitted by: PRAGNAYA RAINA

Registration no.: 3024020012

Under the guidance of

Dr. BONAMALI PAL

Professor

Department of Chemistry and Biochemistry (DCBC),

Thapar Institute of Engineering and Technology

Patiala, 147004

Punjab, India

DECLARATION

I hereby declare that the work being presented in the thesis entitled, "**Photocatalytic hydrogen production from biomass under solar irradiation**", submitted to the **Department of Chemistry and Biochemistry**, Thapar Institute of Engineering and Technology, Patiala, in partial fulfillment of the requirements for the award of the degree of **Master of Science in Chemistry**, is a record of my work that I conducted from January 2026 to July 2026 under the supervision of **Dr. Bonamali Pal**. The results contained in this dissertation have not been submitted in part or full to any other university or institute for the award of any other degree or diploma.

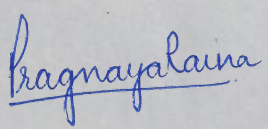

Signature of Candidate

Pragnaya Raina

Registration no. 3024020012

Place: Patiala, Punjab

Date: 24/07/2026

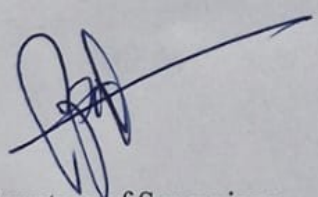

Signature of Supervisor

Dr. Bonamali Pal

Professor

Department of Chemistry and Biochemistry

Thapar Institute of Engineering and Technology, Patiala

Place: Patiala, Punjab

Date: 24/07/2026

CERTIFICATE

This is to certify that the dissertation entitled "**Photocatalytic hydrogen production from biomass under solar irradiation**" being submitted by **Ms. Pragnaya Raina (Roll no. 3024020012)** to the **Department of Chemistry and Biochemistry, Thapar Institute of Engineering and Technology, Patiala**, in partial fulfillment of the requirements for the award of degree of the **Master of Science in Chemistry**, is an authentic record of the work carried out by the candidate under my guidance and supervision. She has fulfilled the requirements for the submission of this dissertation, which, to our knowledge, has reached the requisite standard. The results embodied in the dissertation have not been submitted in part or full to any other university or institute for the award of any other degree or diploma.

Dr. Bonamali Pal

Professor

Department of Chemistry and Biochemistry

Thapar Institute of Engineering and Technology, Patiala

Place: Patiala, Punjab

Date: 24/07/2026

ACKNOWLEDGEMENT

I would like to express my sincere gratitude to my supervisor **Prof. Bonamali Pal** for his invaluable guidance, support and inspiration throughout this research. His unwavering support and willingness to provide all the resources as well as insights drawn from his years of expertise in the research helped me successfully complete this project.

I also extend my gratitude to the **Department of Chemistry and Biochemistry (DCBC) at Thapar Institute of Engineering and Technology** for their facilities and support during this project and **Prof. Manmohan Chibber**, HOD DCBC. The financial and technical support from **DST-FIST** program and **Department of Physics & Material Science (DPMS)** was indispensable during the course of research.

My heartfelt thanks and appreciation to **Ms. Samridhi Kochar** (PhD research scholar) for her unflinching support and patience, helping me navigate through every single road-block during my M.Sc. Dissertation project, without which I wouldn't have been able to give out my best. Much obliged to **Ms. Kirti Bisht** (PhD research scholar) and all of my **lab-mates** for their resolute backing and motivation. I'm grateful for my **friends** Alankrita, Richa, Sukhleen and everyone else, I may have inadvertently omitted, for helping me through moments of frustration and hold ground when in need to meet targets.

Finally, and most importantly, I would like to express my infinite gratitude, to the people who mean the world to me, my **parents** and my **sibling**, for their endless sacrifices, unwavering faith, unconditional love and constant encouragement. I owe this accomplishment and many more to come, entirely to them.

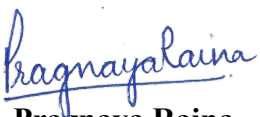

Pragnaya Raina

Date: 30-07-2025

Place: Patiala

TABLE OF CONTENTS

ABSTRACT

This study aimed at finding ways to harvest hydrogen as sustainable fuel from renewable source using clean and abundant solar energy. Sawdust, a renewable and waste material was used for H_2 production, which categorises the harvested hydrogen as 'green hydrogen'. Initial hydrothermal valorisation of sawdust yielded us cellulose, which was used as the sacrificial agent. Sacrificial agent was then photo-reformed to hydrogen using photocatalyst TiO_2 photo-deposited with Au, coated with rGO. TiO_2, Au and rGO being non-toxic and environmentally friendly didn't hamper the 'green' hydrogen production. TiO_2, a semiconductor has band gap of approximately 3.2 eV, which renders it an effective photocatalyst. Nevertheless, its effectiveness is hindered by the rapid recombination of electron-hole pairs. To overcome this, Au of (1,3,5) wt. percentage was photo-deposited onto TiO_2, as metal deposition enhances charge separation. Au also exhibits surface plasmon resonance (SPR), improving light absorption. Among the different loadings tested, 3% Au proved to be the most effective, increasing efficiency without obstructing active sites. Modification of metal loaded photocatalyst with rGO, which is conductive material with π conjugation, helps in further reduction in recombination of electron and holes, this increases the photocatalytic activity, with its best performing wt. % was 10% rGO out of 5, 10 & 12 wt. % rGO on 3% Au-TiO_2. Furthermore, the use of biomass, sawdust as sacrificial agent is great aid for activity enhancement, as it is oxidised by photo-generated holes which reduces the recombination rate also increasing the quantum yield of photo-catalytically produced green H_2. The research successfully illustrated biomass photo-reforming into green hydrogen, yield up to 296.12 mmol, as verified by gas chromatography.

Keywords: Green hydrogen, Sawdust biomass, photoproduced hydrogen, metal photo-deposition, rGO-Au-TiO_2 nano-composite, Biomass photo-reforming

LIST OF ABBREVIATIONS

CB: Conductive Band

DI: Deionized

DRS: Diffuse Reflectance Spectroscopy

GHG: Greenhouse Gas

IPA: Isopropyl Alcohol

JCPDS: Joint Committee on Powder Diffraction Standards

LSPR: Localized Surface Plasmon Resonance

rGO: Reduced Graphene Oxide

VB: Valence Band

XRD: X-ray Diffraction

LIST OF SYMBOLS

Ag: Silver

Au: Gold

CH_4: Methane

CO_2: Carbon dioxide

H_2: Hydrogen

H_2O_2: Hydrogen peroxide

$KMnO_4$: Potassium permanganate

NaOH: Sodium hydroxide

TiO_2: Titanium dioxide

LIST OF UNITS

ºC: Degree Celsius

g: Gram

h: Hour

kV: Kilovolt

mg: Milligram

min: Minute

mL: Millilitre

nm: Nanometre

ppm: Parts per million

rpm: Revolutions per minute

µL: Microlitre

µmol: Micromole

wt.%: Weight percent

Chapter 1 INTRODUCTION AND LITERATURE REVIEW

1.1 INTRODUCTION

1.1.1 Energy Dilemma

The world we live in today, runs on energy, by the fuel of yesterday, which might end up just by tomorrow. The fiasco of attempts to mitigate climate issues, by using clean fuel like hydrogen, is based on the deriving the fuel using fossil fuel itself.

No one who is fully aware of their surroundings is alien to the climate troubles the world has been facing now, from aggravated rage of nature to the depleting quality of life due to destruction of pure natural resources. All of these, in the direct or indirect way are linked to the energy resources that the world has been relying on since the Industrial Revolution.[1,2] Apart from the daily life discomfort caused by fossil fuel, like pollution and degradation of natural resources, there is yet another scare lingering over the humanity, which is the depleting fossil fuel bank.[2] Nonetheless, the uneven concentration of fossil fuel resources in the world has historically led to numerous events of geopolitical instability,[2] a fact made newly visible is the recent-ongoing energy crisis, in the year 2026, due to power clashes in the Middle Eastern area, where $1/5^{th}$ of the world relies on energy for.

This dilemma of dwindling energy supply, concentrated ownership and mounting environmental cost has begun the search for a cleaner, abundant and well distributed energy carrier. This search is what led to the start of this thesis work.

1.1.2 Understanding Fossil fuels and the issue with it

Fossil fuels are a group of primary energy sources that include coal, petroleum, bitumen and their relatives, which are formed by fossilized plants and animals, i.e. organic matter, over millions of years, hence composed of mainly carbon.[3] The energy derived from fossil fuels is by their combustion, which releases harmful amount of CO_2 and other greenhouse gases. The amount of greenhouse gases today in 2026, compared to pre-industrial revolution era, has risen up by over 50% for CO_2 and as much as 170% for CH_4, with the average global temperature rise of 1.3 ºC.[4]

1.1.3 Turn towards Green Energy

Awareness about the cost of using fossil fuel has led towards push for green energy. Green energy also stands for renewable energy, it is generated from renewable sources like solar, wind, geothermal and biomass; which is replenished naturally with least environmental effect.[5] The above-mentioned energy sources are often not continually available and hence require conversion into secondary energy carriers, readily usable at any time.

Among the secondary energy carriers, for eg. methanol, electricity, ammonia, hydrogen etc. H_2 has the most promising return, with its prominent quality being possessing highest gravimetric energy density (120 to 142 MJ/kg) than any conventional fuel.[6] Also owing to the fact that H_2 upon combustion produces only water and no GHG due to it being a non-carbon fuel.[6] H_2 can, in principle, be produced anywhere on the planet given the pre-requisites like water are present there, which decentralises energy production with better energy access. The properties of H_2 as a fuel to have zero carbon emission, high energy density and geographic independence aligns it with seven of the total seventeen Sustainable Development Goals as well.

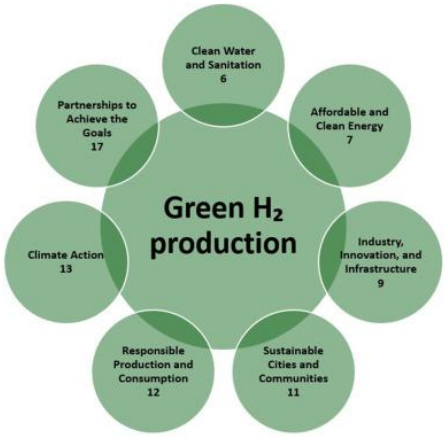

Fig 1: *Seven out of the seventeen Sustainable Development Goals (SDG) green H_2 production aligns with.*

However, for now, it remains a dream to fully realise the dream of 'green hydrogen' fuel, largely due to two reasons. The first is, H_2 is the lightest and smallest atom, which is difficult to store and transport,[7] although solutions like metal hydride transport or the use of multi-layered carbon fibre containers just as in case of what Indian Railways is using for the very first H_2 train in India, are there. Second one is, to produce H_2 as 'green' H_2, which purely depends on the method used for H_2 production.

1.1.4 Routes for H_2 production and the colour spectrum

The various methods for H_2 production with environmental impact are:

- Steam methane reforming (SMR):[8] It is fossil fuel-based method developed in 1930. The hydrogen production is dependent on the use of methane and CO_2 is produced as a byproduct, adversely affecting climate change.
- Electrolysis:[8] This method involves the production of hydrogen through the splitting of water by passing current through it, it produces H_2 and O_2. The carbon footprint is dependent on the source of electricity, if it is renewable source then green hydrogen.
- Thermochemical splitting:[8] It is based on splitting of water or reforming biomass using high energy sources, like power from concentrated solar light, or even nuclear reactor. The temperature required for this technique can reach up to 1000-2000 °C, hence generate high amount of heat, although it is more affordable than electrolysis technique.
- Biomass:[9] The route of reforming biomass for H_2 is the conventional one, like gasification, which is comparatively eco-friendly but has the disadvantage of low H_2 yield.
- Photocatalytic method:[10] This uses semiconductor catalyst which uses sunlight to reduce activation energy and help in the reforming of biomass or in the lysis of water, in presence of sunlight.

Based on the method of production, H_2 is categorised into various colours:[11]

- Grey: H_2 produced from natural gas via stem reforming method, making this process release CO_2 and GHGs.
- Pink: H_2 generated from water electrolysis, powered by nuclear energy.
- Red: H_2 formed using electrolysis or high temperature catalysis using nuclear energy, correlating to pink H_2
- Blue: H_2 produced from natural gas via stem reforming method, making this process release CO_2, but the CO_2 released is captured and stored, thus lower carbon footprint.
- Yellow: H_2 released from water electrolysis undertaken by solar energy.
- Black: Production of H_2 from the gasification of coal, has the highest carbon footprint.
- Turquoise: H_2 produced through methane pyrolysis, where no CO_2 is released but the gas is split into hydrogen and solid carbon.

- White☁: This includes the naturally occurring geological hydrogen found trapped in underground deposits.
- Green☁: H_2 produced using clean and renewable primary energy sources like solar, wind etc, involves splitting of water or transforming waste like biomass to hydrogen.

The above categorisation talks about the importance of source of H_2 production; therefore, it brings us to the point of importance of choosing biomass instead of classic use of water for the green H_2 production. Moreover, using biomass to photo-reform and generate H_2 from rather than water increases the quantum efficiency, as biomass act as sacrificial electron donor (organic molecule that is oxidized by photogenerated holes) which increase the holes consumption thereby reducing electron-hole recombination, suppressing reverse reaction. [12, 13] The hydrogen hence produced by this route in the experimental system built for this thesis is green hydrogen, by definition and design.

1.1.5 Experimental work

Photocatalytic H_2 production using TiO_2 based semiconductor is quite actively researched area within green H_2 production. TiO_2 remains the most widely used photocatalyst [14, 15] for this reaction because it is stable, have the ability to be activated by solar light inexpensive and resistant to photo-corrosion. In a semiconductor, there exist a valence band and a conduction band, separated by band gap (E_g). [15, 16] Upon incidence of light, the energy of photons when greater than the band gap promotes the electrons to CB from VB, which leaves hole behind in VB. Another important property required for efficiency of semiconductor is the CB to be more negative and VB to be more positive.

As per the properties mentioned, TiO_2 stands, satisfying all except for its huge band gap close to 3.2 eV [15] which resists its absorption in the UV range only. To mitigate this, we doped the photocatalyst with Au first and then modified it further by coating it with rGO nanosheet. These modifications show enhanced photo-catalytic activity due to reduced recombination rate and the increase in absorption in visible light range due to SPR effect of Au, shown in DRS graphs, in the Results and Discussion section.

Metal loading, especially noble metal co-catalyst loading onto semiconductor helps because it creates a Schottky barrier at the metal-semiconductor interface [17, 18], trapping the photoexcited

electrons, which suppress recombination. It also introduces prior mentioned SPR effect which shifts the absorption spectrum to visible range. [18, 19]

Reduced graphene oxide, rGO, improves charge separation in TiO_2[20, 21] by taking the photoexcited electrons to its conjugated π-system. The ternary catalyst thus formed with metal co-catalyst and rGO demonstrated better H_2 production capacity than the binary composite formed.

Moreover, the most significant development in the research done in this thesis was using complex substrate cellulose for photo-reforming [22, 23], rather than the use of alcohol etc. Cellulose was initially derived from genuine, un-refined biomass, with which the research is still ongoing, but even with commercial micro-crystalline cellulose, we were able to produce green H_2 in this research work.

1.1.6 Why sawdust and how was it used?

Sawdust was selected as the lignocellulosic feedstock for the present study because it is an abundant and low-cost waste generated by wood-processing activities and provides a cellulose-rich renewable carbon source. Its utilization for photo-reforming also offers the possibility of coupling waste valorisation with the production of value-added products such as hydrogen.[38] However, the compact lignocellulosic structure of sawdust, in which cellulose is associated with lignin and hemicellulose, limits the accessibility of cellulose and therefore requires an appropriate pretreatment step.[39] Several approaches have been reported for cellulose isolation, including acid and alkaline treatments, organo-solv processes, oxidative delignification, ionic liquids, deep eutectic solvents, and physical-assisted methods such as microwave and ultrasonication[40]. In the present work, cellulose was isolated through NaOH-assisted hydrothermal treatment followed by H_2O_2 bleaching. Alkaline conditions of NaOH facilitates the removal of lignin and hemicellulose, disrupting the lignocellulosic matrix, whereas oxidation by H_2O_2 further promotes delignification and bleaching, thereby enriching the cellulose fraction [41, 42]. Compared with processes employing strong mineral acids, chlorine-containing bleaching agents, or organic-solvent-based fractionation, the adopted NaOH-H_2O_2 route represents a comparatively simpler and potentially greener approach because it avoids chlorinated bleaching chemicals and extensive organic-solvent use, while H_2O_2 ultimately decomposes to water and oxygen [41, 42]. Thus, the treatment provides a practical route for

converting waste sawdust into a cellulose-rich substrate suitable for subsequent photocatalytic reforming.

1.1.6 Research gaps

1) Attempt to counter the realism gap in research by utilizing complex organic substrate, and ongoing research on biomass-derived complex substrate.

2) Utilizing the less explored Au loaded TiO_2 coated with rGO ternary composite and using it for biomass derived sacrificial agent.

1.2. LITERATURE REVIEW

Photocatalytic water splitting for hydrogen production was first demonstrated by Fujishima and Honda [1972][24] using TiO_2 electrodes, which established semiconductor photocatalysis on the pedestal to generate green hydrogen. TiO_2 since then has been established as the most stable, and benchmark photocatalyst. But its huge band gap created inconvenient and low h_2 yields due to high recombination rate. Further research to overcome this limitation were undertaken, which found out that using sacrificial hole scavengers like organic substrates [12, 25] are oxidised by photo-generated holes, which significantly reduce the recombination rate. Initially scavengers like methanol i.e. simple alcohols were only used [26], which later on was extended to using biomass-derived substrates [13, 27] Furthermore, it was found that metal loaded semiconductor with scavengers enhanced the photocatalytic water splitting more. The metal loading was done using noble metals like Pt, Pd, and Au; [17, 26] these introduced Schottky barrier and enhanced the activity. During 1980s and 1990s, research was concentrated on pure water splitting using TiO_2. But the rapid recombination of photogenerated electron-hole pairs in TiO_2 due to large band gap shifted the research to make efficient photocatalysts which had smaller band gap which could further help in better harvesting the visible light. Later in 2000s the researchers did their work shifting the H_2 production from water splitting to simpler biomass-derived precursors like ethanol and sugar [28]. Also, research for better catalysts shifted the focus from TiO_2 based to metal sulphide based like CdS etc. [29, 30] During 2010s there was transition phase where the photocatalyst like noble metal doped TiO_2 was investigated, as the photocatalytic activity enhanced due to Schottky barrier [19, 31]. Also, in the late 2010s researchers tried to use biomass derived complex molecules for green hydrogen production. [22, 29, 32]

As per the current scenario, researchers have been trying to inculcate the use of materials like gCN, GO along with biomass derived complex materials [19, 30, 33, 34, 35, 36, 37]

1.3. OBJECTIVES

1) Extraction of complex bio-polymer cellulose from earth abundant waste - sawdust, in relatively mild conditions, further attempt to convert it to hydrogen, as waste to wealth.

2) Preparation and activity study of photo-deposited TiO_2 nanoparticles with noble metals Au and Ag, to choose the most efficient composite for photocatalytic reforming. Later performing the weight studies with the most efficient photocatalyst.

3) Synthesis and characterisation of Au-TiO_2 coated with weight optimized rGO nanosheet.

4) To study the photocatalytic reforming of cellulose with Au-TiO_2 coated with rGO nanosheet under solar irradiation, to produce H_2, a clean energy source aligning with the sustainable development goals (SDG).

Chapter 2 EXPERIMENTAL DISCUSSION

2.1 EXPERIMENTAL SECTION

2.1.1 Apparatus required

Argon gas cylinder, Bead picker, Beakers, Centrifuge, Centrifugation tubes, Conical flasks, Crucible, Double sided wrench, Droppers, Drying oven, Gas chromatograph, Hypodermic needle, Magnetic beads, Measuring cylinder, Micro-centrifuge tube, Micro-pipette, Micro-syringe, Muffle furnace, Parafilm, Petri dishes, pH meter, Rubber septa, Spatula, Stirrer, Teflon lined autoclave, Test tubes, Test tube stand, Weighing balance, UV-visible photoreactor.

2.1.2 Chemicals required

Acetic acid (CH_3COOH), Chloroauric acid ($HAuCl_4$), Distilled water, Ethanol (C_2H_5OH), Graphite powder, Hydrazine monohydrate ($NH_2NH_2.H_2O$), Hydrochloric acid (HCl), Hydrogen peroxide (H_2O_2), Methanol (CH_3OH), Micro-crystalline cellulose, Potassium permanganate ($KMnO_4$), Sawdust, Sigma-Aldrich Titanium dioxide (TiO_2), Sodium chloride (NaCl), Sodium hydroxide (NaOH), Sodium nitrate ($NaNO_3$), Sulphuric acid (H_2SO_4).

2.2 METHODOLOGY

2.2.1 Extraction of cellulose from sawdust

In a beaker, 10 g locally sourced waste i.e. sawdust was mixed with 1:20 ratio NaOH and DI water solution.[41] The solution was stirred for 10 min and then transferred to Teflon-lined autoclave, which was kept in the hydrothermal for 3 h @ 180 °C. Once the hydrothermal valorisation was over, the hydro-tar was separated and washed @6000 rpm. Washed product

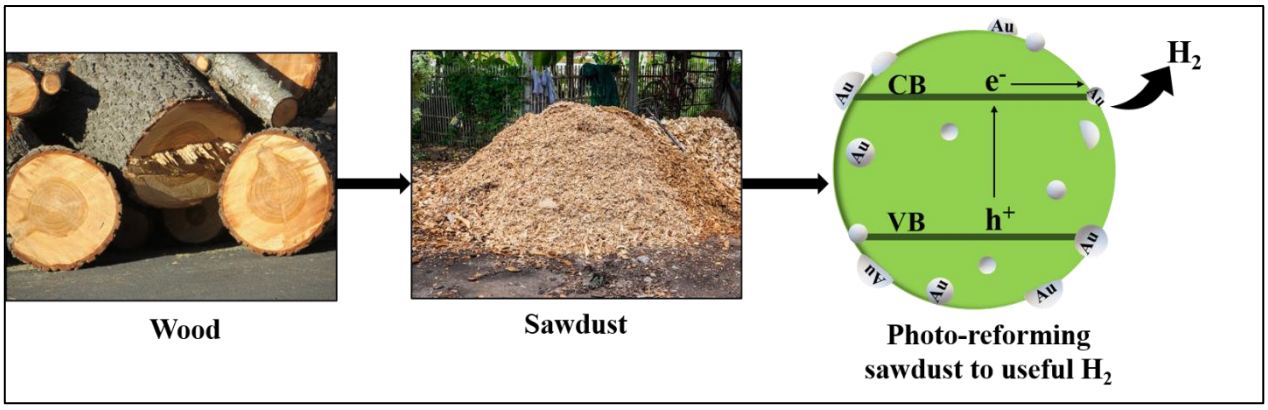

Fig 2.1: *Photo-reforming sawdust-a biomass waste to useful-H_2*

was neutralized and subsequently oxidised using H_2O_2 30% solution. [19, 41, 42] The obtained mass was washed again, thrice, @ 6000 rpm with DI water, and later kept for drying @ 60 °C for 12 h. [19]

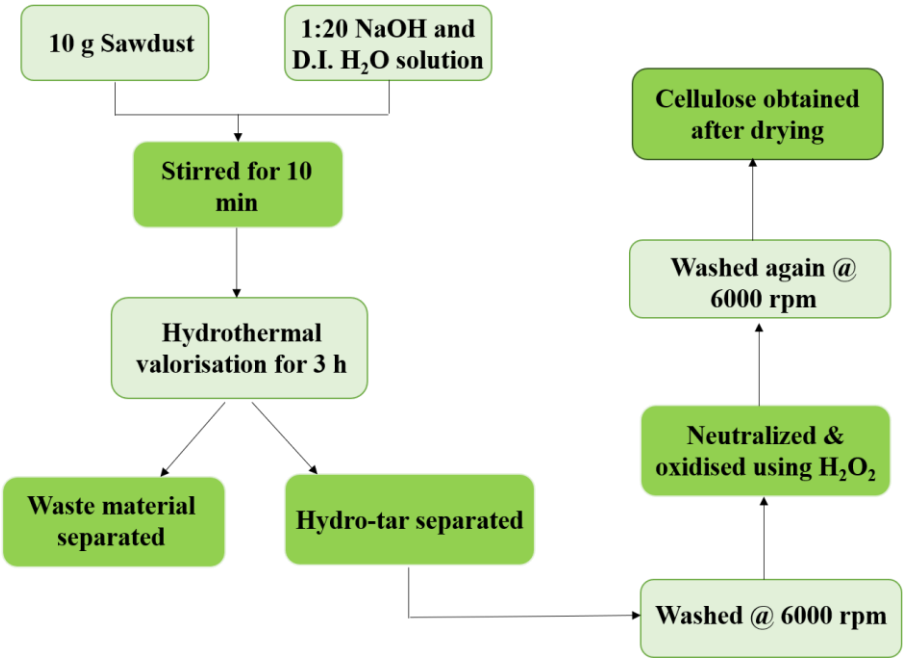

Fig 2.2: *Route of extracting cellulose from sawdust through hydrothermal valorization.*

2.2.2 Synthesis of Ag-TiO_2

In each test tube at a time, 100 mg of Sigma-Aldrich TiO_2 was taken, to which 0.01 M solution of silver nitrate (10.7 mg silver nitrate in 10 ml DI water) was added in µl volume using a micro-pipette. For different weight percentages, the volume varied as, 927 µl for 1%, 2781 µl for 3% and 4635 µl for 5% Ag deposition. To the test tube, further 5 ml IPA and 5 ml DI water was added. The test tubes were sealed and further purged with Ar gas for 15 min. For the photo-deposition of Ag on TiO_2 the solutions prepared were kept in UV-Vis chamber with constant stirring for 2 h. After 2h, the obtained solution was collected in centrifuge tubes and centrifuged @ 6000 rpm, with 2 subsequent DI water washing and 1 ethanol washing. Finally, the nanocomposite obtained was kept for drying in the oven @ 60 °C for 12 h. [36, 37]

2.2.2 Synthesis of Au-TiO_2

In each test tube at a time, 100 mg of Sigma-Aldrich TiO_2 was taken, to which 0.01 M solution of chloroauric acid (34 mg chloroauric acid in 100 ml DI water) was added in µl volume using a micro-pipette. For different weight percentages, the volume varied as, 507.4 µl for 1%, 1522.2 µl for 3% and 2537 µl for 5% Au deposition. To the test tube, further 5 ml IPA and 5 ml DI water was added. The test tubes were sealed and further purged with Ar gas for 15 min. For the photo-deposition of Au on TiO_2 the solutions prepared were kept in UV-Vis chamber with constant stirring for 2 h. After 2h, the obtained solution was collected in centrifuge tubes and centrifuged @ 6000 rpm, with 2 subsequent DI water washing and 1 ethanol washing. Finally, the nanocomposite obtained was kept for drying in the oven @ 60 °C for 12 h. [36, 37]

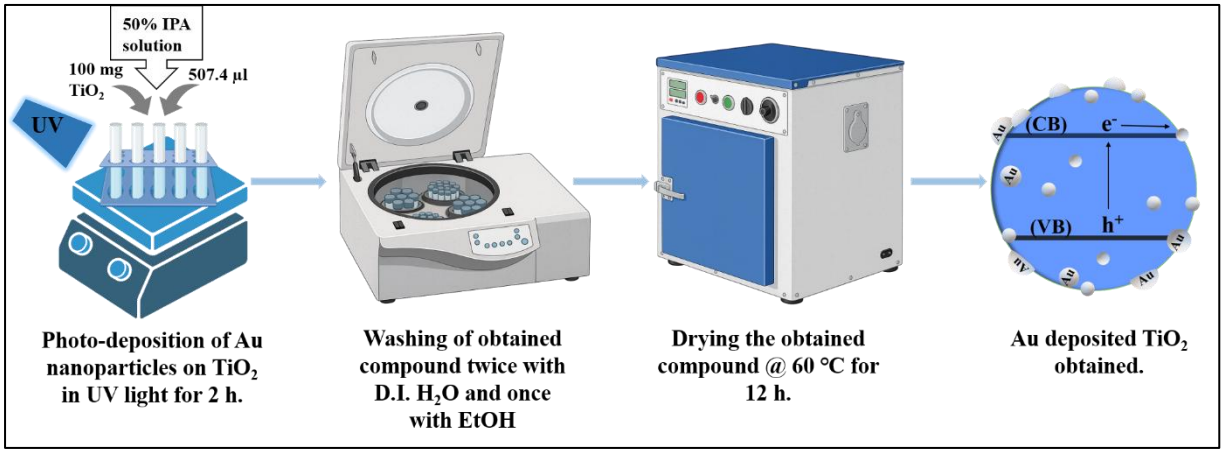

Fig 2.3: Photo-deposition of Au on TiO_2

2.2.3 Synthesis of GO (Graphene oxide)

The synthesis was done using modified Hummer's method in which graphite powder was stirred for 4 h with $NaNO_3$ and conc. H_2SO_4 in an ice bath, followed by gradual addition of $KMnO_4$ in 10 min. Further DI water was added to the solution and it was stirred for 2 h. The mixture was heated to 90 °C and stirred for 2h, the stirring was made to stop after the addition of 100 ml DI water. The reaction was made to stop by adding 30% H_2O_2. A 5% HCl solution was used to wash the mixture and was allowed to settle down for 1 day. The suspension was washed with DI water and dried @ 60 °C.

2.2.4 Synthesis of rGO (reduced Graphene oxide)

1 mg/ml of graphite dispersion (100 ml) was mixed with hydrazine monohydrate (1 ml) and mixture for stirred @ 80 ℃ for 3h. Once reduction was complete, the suspension was filtered, repeatedly washed with D.I. water and then dried @ 60 ℃ for 1 day. [35]

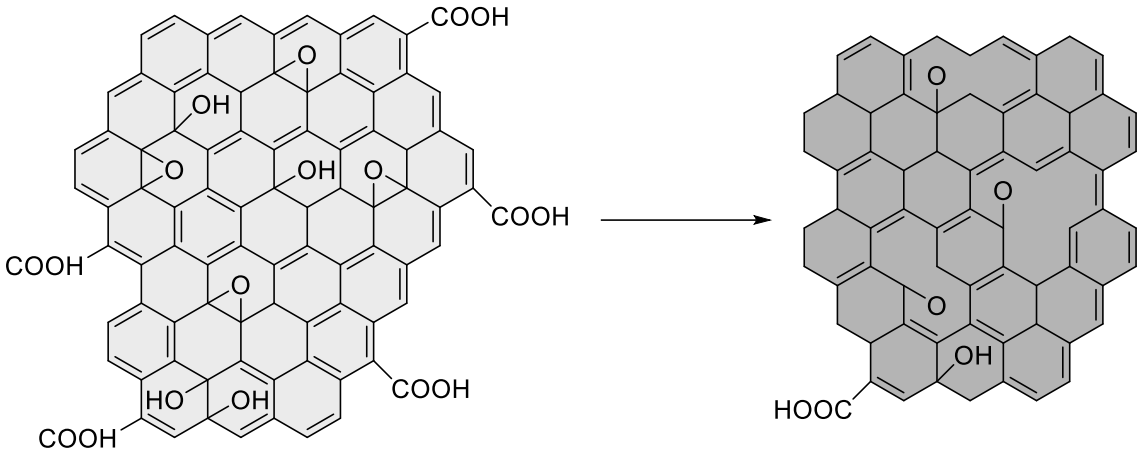

Graphene Oxide **Reduced Graphene Oxide**

2.2.5 Synthesis of rGO @ 3% Au-TiO_2

5 mg of rGO was added to 20 ml, 1:2 ethanol and water solution, which was made to sonicate for 15 min. Then 100 mg 3% Au-TiO_2 was added to the solution and further sonicated for 15 min. The solution was transferred to a Teflon-lined autoclave, kept in hydrothermal for 1 h @ 180 ℃, and later the obtained solution was centrifuged @ 6000 rpm, washed twice with D.I. water and once with ethanol, finally kept for drying @ 60 ℃ for 12 h. [35, 36]

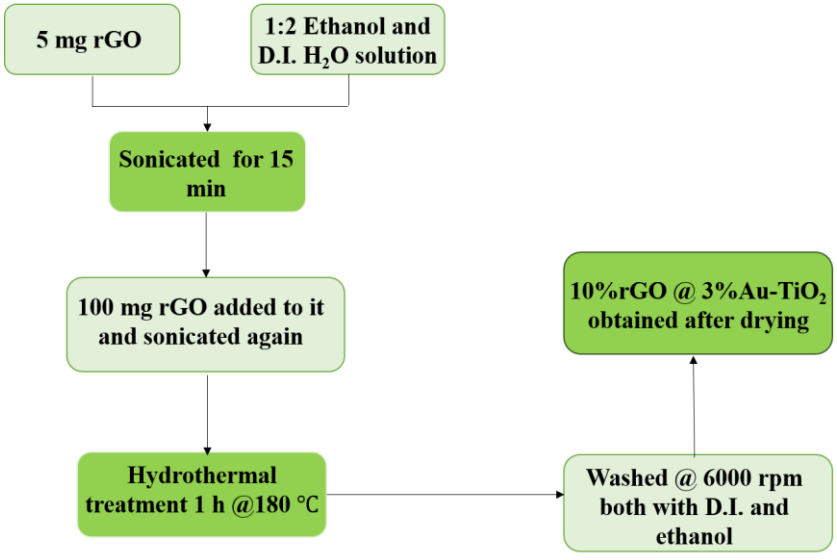

Fig 2.4: Synthesis mechanism of final composite 10%rGO 3%Au-TiO_2

2.3 CHARACTERISATION METHODS

A range of characterization techniques were employed to evaluate the structural and physico-chemical properties of the prepared catalysts.

For the structural/crystallographic studies, XRD PANanalytical-X'pert-PRO machine was used, using Cu-Kα radiation source (1.54 Å) running @ 45kV with a diffraction angle (2θ) ranging from 10º-80 º scan rate. XRD works on the principle of Bragg's Law, which governs the relationship between diffraction angles and interplanar spacing, in it X-rays interact with atomic lattice of material, producing a characteristic diffraction pattern which is used to identify the crystal structure and phase.

Morphological and elemental studies were undertaken by using FE-SEM and EDS. FE-SEM (Carl-ZEISS Sigma 560 VP) which stands for Field Emission Scanning Electron Microscopy, works on the principle of scanning the material with finely focused field-emitted electron beam over to produce high-resolution images from the emitted secondary and backscattered electrons. EDS (Bruker EDS) which stands for Energy Dispersive X-ray Spectroscopy, works on the principle of identifying and quantifying the characteristic X-rays emitted from atoms after electron beam excitation.

The structural and chemical characterization was done using Raman and FTIR techniques. For Raman, Horiba micro-Raman Spectrometer (Labram HR) with 532 nm laser excitation was used and it is based on the inelastic scattering known as Raman scattering of the monochromatic light, which provides information about the molecular vibrations and crystal structure of a material. FTIR done using Agilent FTIR spectro-photometer, stands for Fourier Transform Infrared Spectroscopy is based on the principle of absorption of infrared radiation by molecular bonds, which produces characteristic vibrational spectra helping us identify the functional groups present in a material.

Furthermore, optical characterization was done employing UV-Vis DRS (Jasco, V-750), it is abbreviation of Diffused Reflectance Spectroscopy. It is based on the measurement of diffusely reflected UV-Vis light from a material which helps us determine the optical absorption properties and the band gap energy. It requires a reference to study the material's properties with respect to and in the analysis, $BaSO_4$ was taken as the reference material to set the baseline with.

2.4 PHOTOCATALYTIC HYDROGEN PRODUCTION

The photocatalytic hydrogen production from the photocatalytic reforming of biomass, i.e. micro-crystalline cellulose, using initially 1% Ag and 1% Au TiO_2 were studied, as $AuTiO_2$ performed better so various wt.% of Au-TiO_2 and then different wt. % rGO coated Au-TiO_2 nano-composites were studied.

A 25 ml conical flask sealed with rubber septa containing 80 mg catalyst, 150 mg cellulose, 20 ml water and 2 ml ethanol as a hole scavenger (co-substrate) was added for photocatalytic reforming. The solution was purged with Ar gas for 15 min, which was then kept for irradiation under sunlight (Intensity range = 900-1300 W/m^2) for 5 h.

For the analysis of the amount of H_2 produced, GC (Nucon India) with (5X A column) molecular sieve and Ar as carrier gas was used. A gas-tight Hamilton micro-syringe was used to inject 1µl gas into the injector port. The temperature of TCD and injector was set at 50 ℃ and 40 ℃, respectively, while the temperature off the column was kept at 40 ℃. The GC chromatograms were measured against standard hydrogen concentration of 505 ppm. The peak height of H_2 is shown in gas chromatograms with the retention time between 00:30-00:75, min:sec. The general formula for the solar to hydrogen conversion rate is given below:[19]

$$\text{STH\%} = \frac{Rate\ of\ H_2 \times \Delta G}{Surface\ \ area\ of\ reactor \times Solar\ flux}$$

$here,\ \Delta G\ (Gibbs\ free\ energy)$ = 273 KJ/mol

2.4 PHOTOCATALYTIC HYDROGEN PRODUCTION

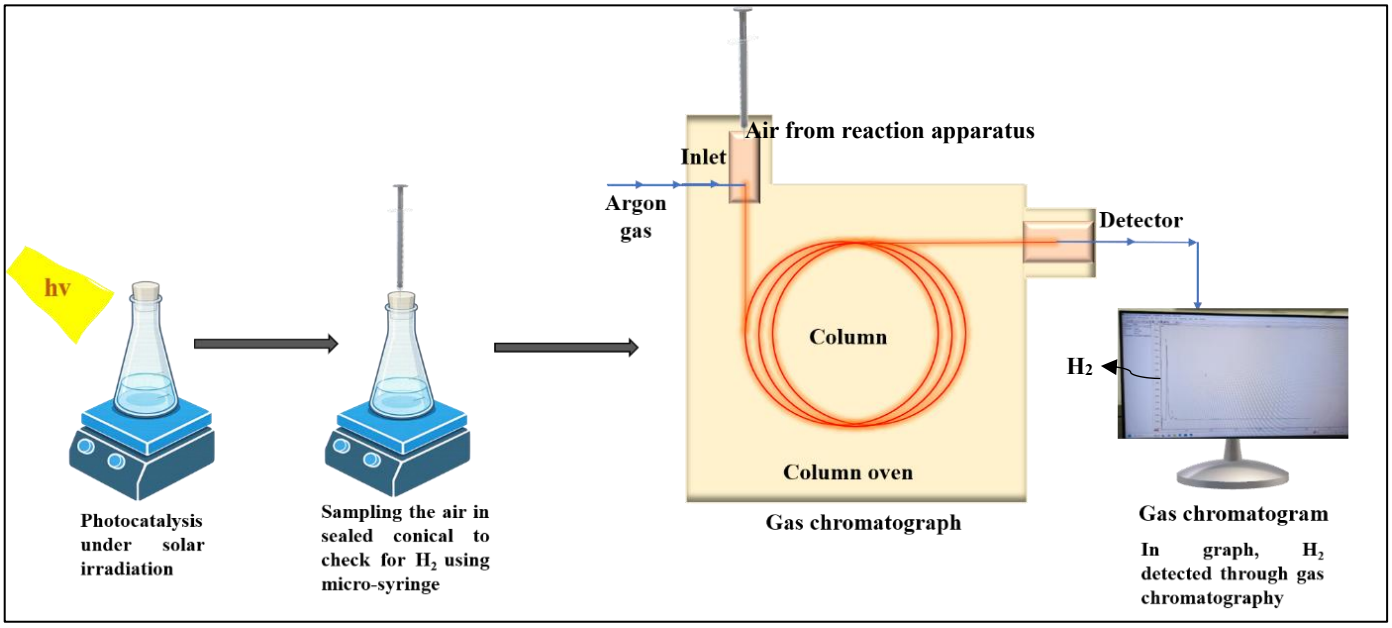

Fig 2.5: Photocatalytic H_2 production

2.5 PROPOSED PHOTOCATALYTIC MECHANISM

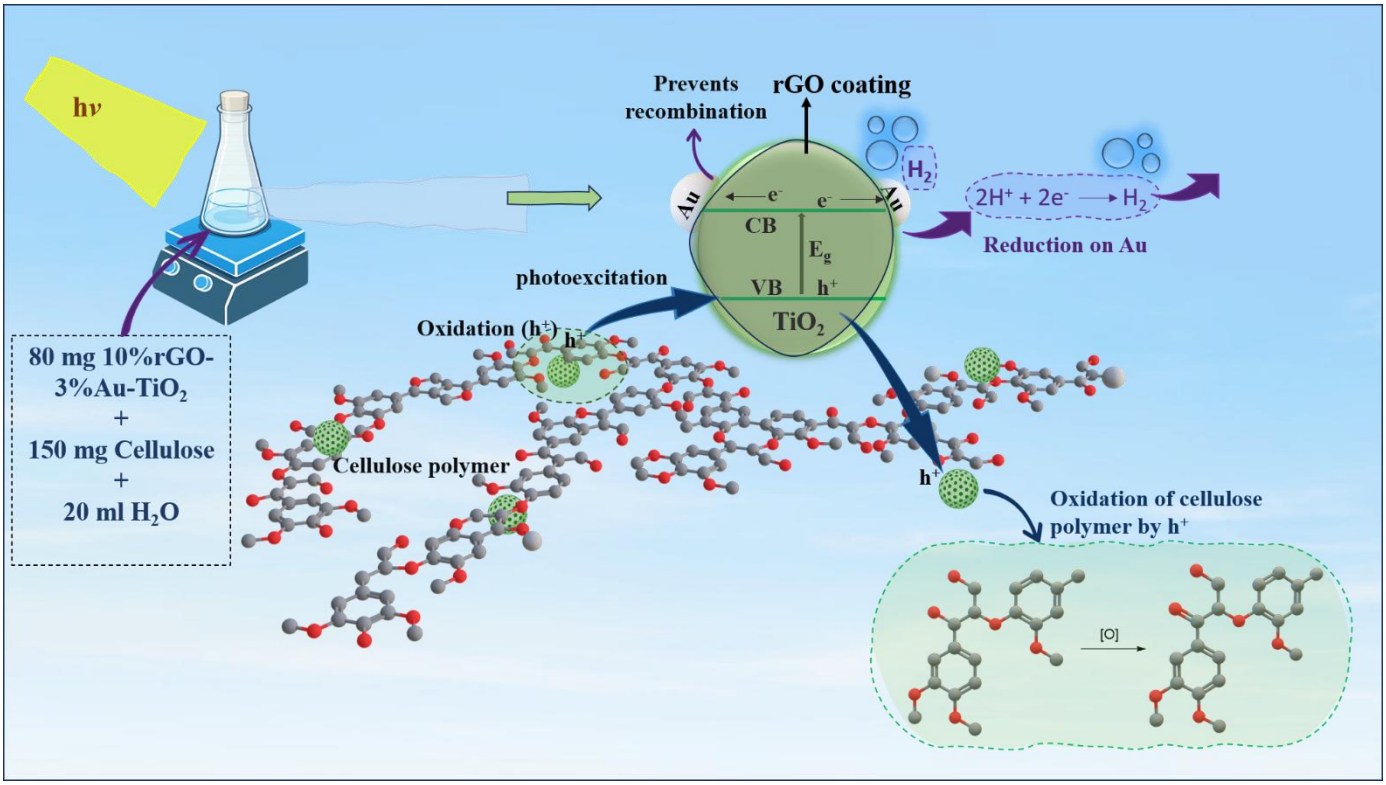

3.1 CHOOSING THE METAL FOR DOPING THE CATALYST

During the initial photocatalytic screening under sunlight irradiation, 1% Au-TiO_2 was selected over 1% Ag-TiO_2 owing to further investigation of its comparatively higher hydrogen production. Under identical experimental conditions and exposure to sunlight for 5 h in the intensity range of 900-1300 W/m^2 during the month of June 2026 in Patiala, Punjab, and it was observed that 1% Au-TiO_2 produced 19.43 µmol of H_2, whereas 1% Ag-TiO_2 yielded 16.91 µmol of H_2.

This higher activity can be due to the favourable interaction between Au nanoparticles and TiO_2. Due to the higher work function of Au, the Au-TiO_2 interface can form an effective Schottky barrier, allowing Au nanoparticles to act as electron traps and thereby reducing the recombination of photogenerated electron-hole pairs. Moreover, the localized surface plasmon resonance (LSPR) effect of Au can enhance the utilization of visible light under solar irradiation and facilitate interfacial charge transfer. [19, 35, 37] Au also possesses greater chemical stability than Ag under photocatalytic conditions, where Ag may undergo surface oxidation that can affect its activity.[35] Therefore, the improved charge separation, plasmonic light absorption, and stability associated with Au-TiO_2 may explain its comparatively higher hydrogen evolution and support its selection for further photocatalytic studies.

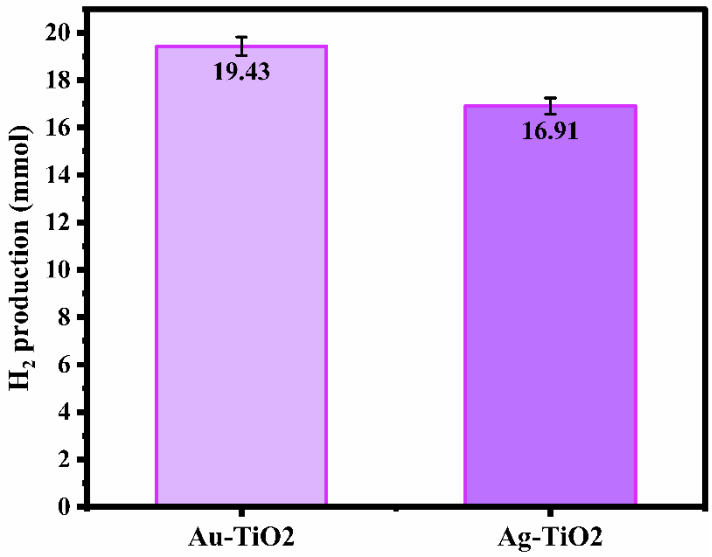

Fig 3.1: *H_2 production of 1% wt. loaded Au and Ag on TiO_2 Activity checked after 5 h of solar irradiation.*

3.2 EXTRACTING CELLULOSE FROM BIOMASS

FTIR

Samples of sawdust and cellulose were investigated using FTIR, which helped in distinguishing both samples by looking into the change of functional groups. The prominent spectral changes observed as in Fig 3.2 and 3.3 are:

At 3300 cm^{-1}, sawdust showed broad absorption band which corresponds to stretching vibrations of hydrogen-bonded OH functional group, this group is an indicator of ligno-cellulosic matter. This broad band was retained in case of cellulose too at 3300 cm^{-1}.

At 2900 cm^{-1}, corresponds to aliphatic C-H stretching and is present in both compounds.

1733 cm^{-1} in sawdust corresponds to C=O stretching of hemicellulose which evidently weakens in cellulose at 1733 cm^{-1}, showing transformation of sawdust.

Then the bands in the fingerprint regions range show weakening from sawdust to cellulose graph, as this region is known to have bands due to lignin or hemicellulose.

Furthermore, the peak at 895 cm^{-1} remains as it is the characteristic peak of cellulose.[42]

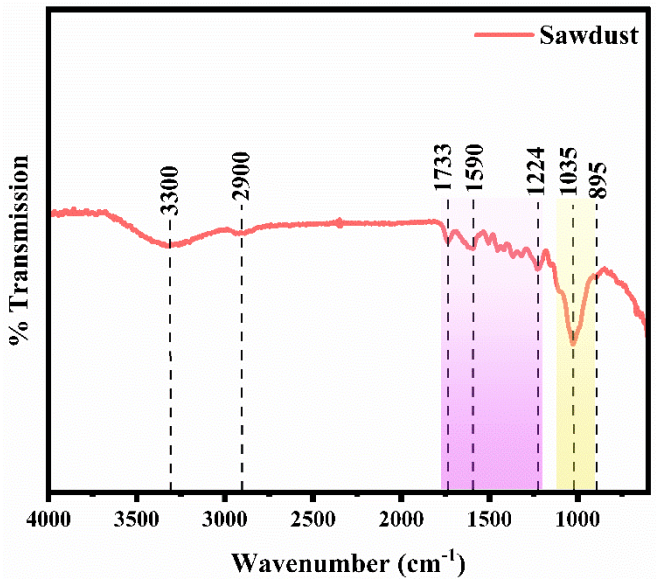

Fig 3.2: FTIR spectra of sawdust.

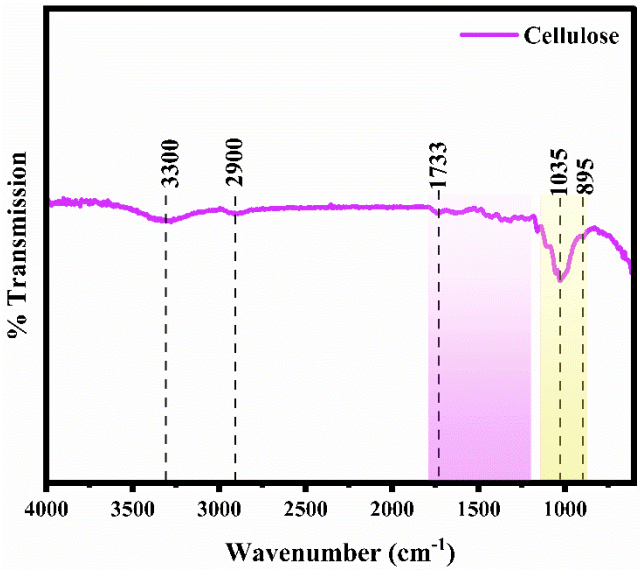

Fig 3.3: FTIR spectra of cellulose.

3.3 CATALYTIC STUDIES AND CHARACTERISATION

XRD

Fig 3.4 shows the XRD spectra of TiO_2 and 3% Au-TiO_2, starting with TiO_2, its XRD spectra is confirmed by the JCPDS Card no. 21-1272. The same spectra is observed in the case of 3% Au-TiO_2, as both samples show sharp diffraction peak at 2θ = 25º, 37º, 48º, 53º, 62º, 68º, 70º, 75º and 82º, which all corresponds to the crystallographic planes: (101); (004), (112), (103); (200); (211); (105); (204); (116); (220); (215) and (224). The data reflects the presence of tetragonal anatase phase of TiO_2, and the sharp peak of 101 crystallographic plane at 25º confirms high degree of crystallinity of TiO_2. However, the distinct peak of Au is absent which is usually present at 2θ = 38º for (111) crystallographic plane,[37] this could be attributed to the low wt.% loading of Au, producing weaker signal to be detected; moreover, the presence of Au is confirmed by other characterisation techniques discussed further.

Fig 3.5 shows the XRD spectra of rGO and 10% rGO @ 3%Au-TiO_2. The XRD pattern of rGO JCPDS Card no. 41-1487 show huge-broad diffraction peak at 2θ = 25º for (002) crystallographic plane and weak-broad diffraction peak at 2θ = 43º for (102) crystallographic plane. [35, 36] The broadening of (002) peak in rGO reflects turbostratic disorder and lesser crystallite domain which is characteristic for rGO, hence confirming its synthesis. However, in the XRD pattern of 10%rGO @ 3%Au-TiO_2 there is absence of the peaks indicating presence of rGO, especially the prominent (002) peak in rGO, this can be attributed to the suppression because of less crystalline nature of rGO and presence of sharp peaks in the spectra of 10%rGO @ 3%Au-TiO_2. [36] Hence confirming the formation of crystalline final photocatalyst. Moreover, the presence of rGO in the final catalyst is confirmed by other characterisation techniques discussed further.

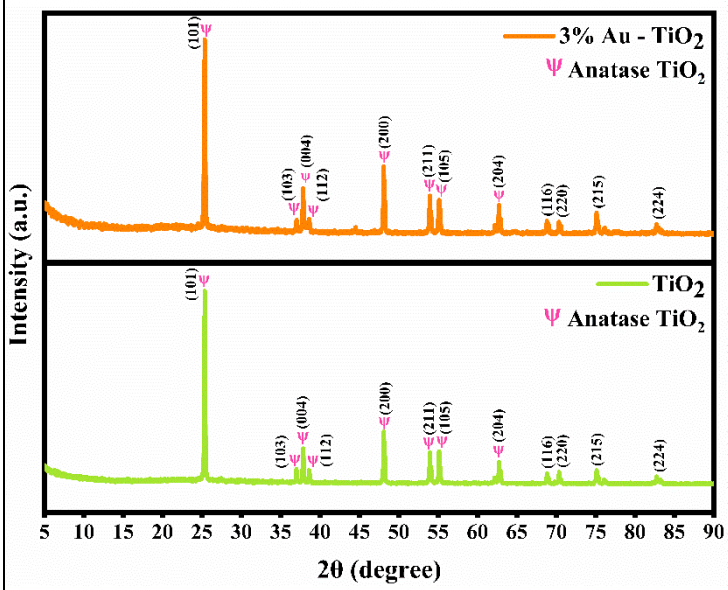

Fig 3.4: XRD spectra of TiO_2 and 3%Au-TiO_2

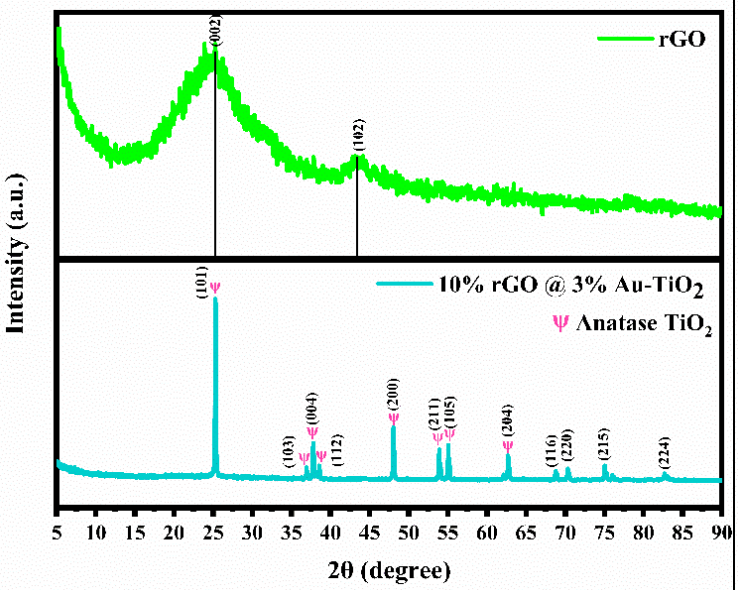

Fig 3.5: XRD spectra of rGO and 10%rGO @ 3%Au-TiO_2

FE-SEM & EDS

FE-SEM was used for the morphological studies of the nano-composite photocatalyst formed and the nano-composites 3% Au-TiO_2 as well as 10% rGO @ 3% Au-TiO_2 were examined at different magnifications. Fig 3.5 shows the surface of 3% Au-TiO_2, which has visible formation of nano-spheres. The elemental composition of 3% Au-TiO_2 was studied using EDS as in Fig 3.5 (b) and it confirms the presence of expected elements, while also detecting the undetected Au in XRD.

Further in Fig 3.6, FE-SEM image showing the surface of 10% rGO@ 3%Au-TiO_2 is seen, which is evidently blurred, confirmed the deposition of rGO nano-sheet over the surface of 3% Au-TiO_2 microspheres. The EDS analysis in Fig 3.6 (b) confirms the presence of rGO in our final prepared nano-composite 10% rGO@ 3% Au-TiO_2

(a)

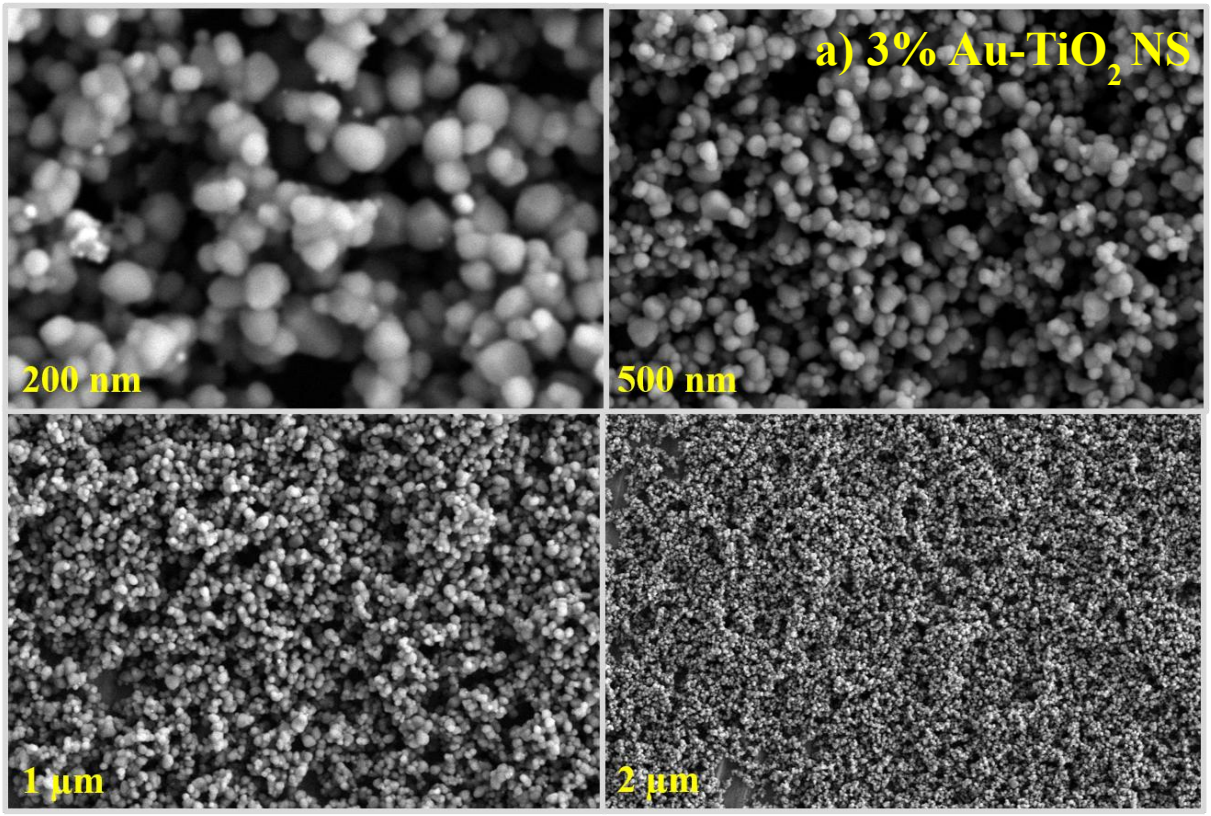

(b)

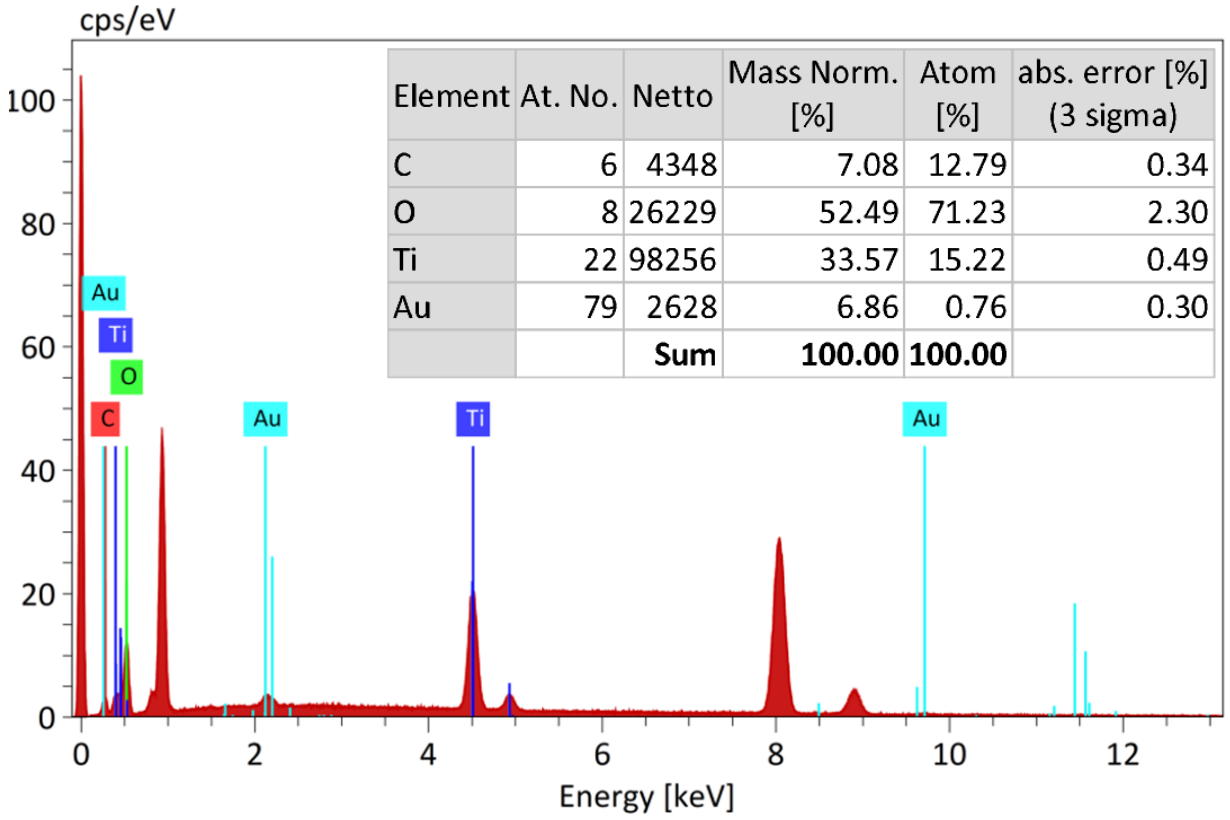

Element	At. No.	Netto	Mass Norm. [%]	Atom [%]	abs. error [%] (3 sigma)
C	6	4348	7.08	12.79	0.34
O	8	26229	52.49	71.23	2.30
Ti	22	98256	33.57	15.22	0.49
Au	79	2628	6.86	0.76	0.30
		Sum	**100.00**	**100.00**	

Fig 3.6 (a) & (b): *(a) FE-SEM image of 3% Au-TiO_2 nano-spheres*

(b) EDS graph of 3% Au-TiO_2.

(a)

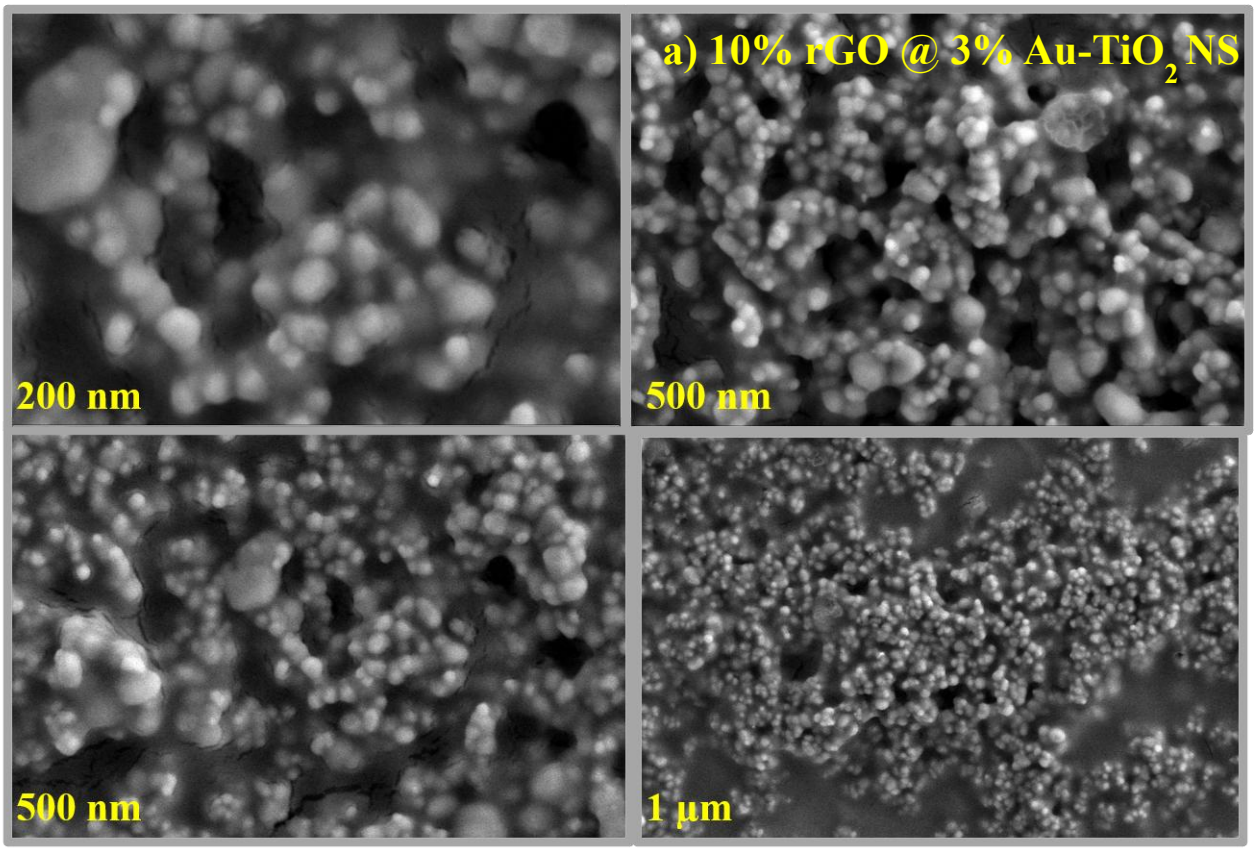

(b)

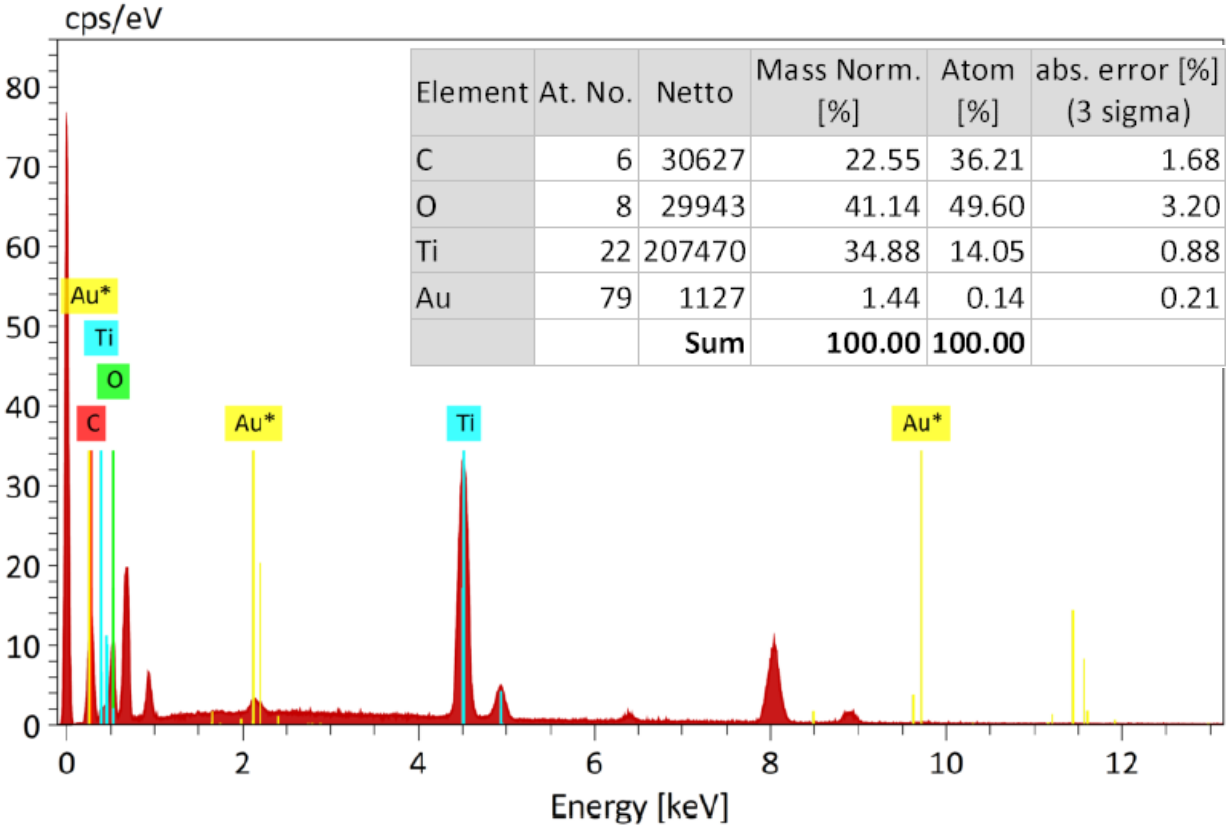

Element	At. No.	Netto	Mass Norm. [%]	Atom [%]	abs. error [%] (3 sigma)
C	6	30627	22.55	36.21	1.68
O	8	29943	41.14	49.60	3.20
Ti	22	207470	34.88	14.05	0.88
Au	79	1127	1.44	0.14	0.21
		Sum	**100.00**	**100.00**	

Fig 3.7 (a) & (b): *(a) FE-SEM image of final compund 10% rGO @ 3% Au-TiO_2 nano-spheres*

(b) EDS graph of 10% rGO @ 3% Au-TiO_2

RAMAN

The Raman spectra of TiO_2, 3% Au-TiO_2, rGO and 10% rGO @ 3% Au-TiO_2 were analysed and all except rGO had prominent peak at 142 cm^{-1}, 398 cm^{-1}, 517 cm^{-1} and 636cm^{-1} for E_g, B_{1g}, A_{1g} and E_g respectively. However the spectra of rGO depicts the presence of D and G bands, which shows structural defect and sp^2 stretching of C atoms, respectively. The spectra of 10% rGO @ 3% Au-TiO_2 also shows the presence of these bands, due to the presence and deposition of rGO. TiO_2 exhibits the characteristic Raman-active modes of anatase at approximately 144 cm^{-1} (E_g), 197 cm^{-1} (E_g), 399 cm^{-1} (B_{1g}), 513–519 cm^{-1} (A_{1g} + B_{1g}), and 639 cm^{-1} (E_g). These bands arise from different lattice vibrations of the TiO_6 octahedral framework; in particular, the E_g modes are mainly associated with symmetric O-Ti-O vibrations, whereas the B_{1g} and A_{1g} modes originate from bending and stretching vibrations within the anatase lattice. [35, 37]

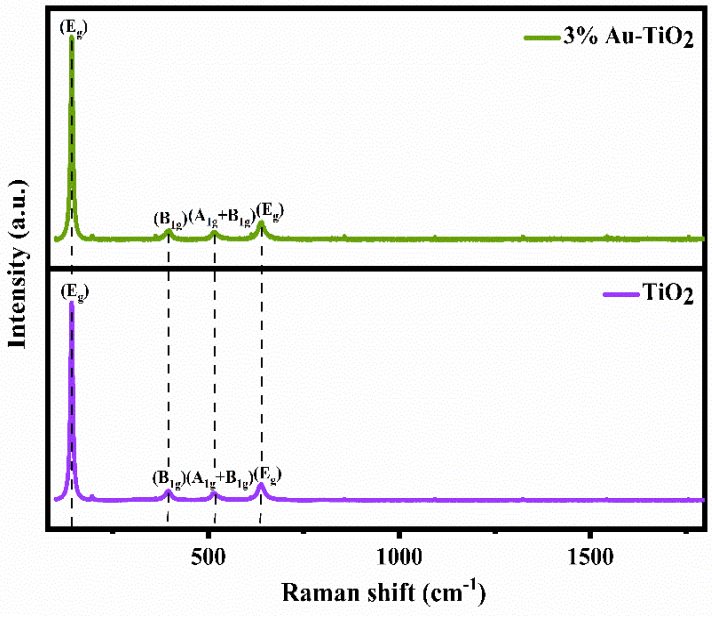

Fig 3.8: Raman of 3% Au-TiO_2 and TiO_2

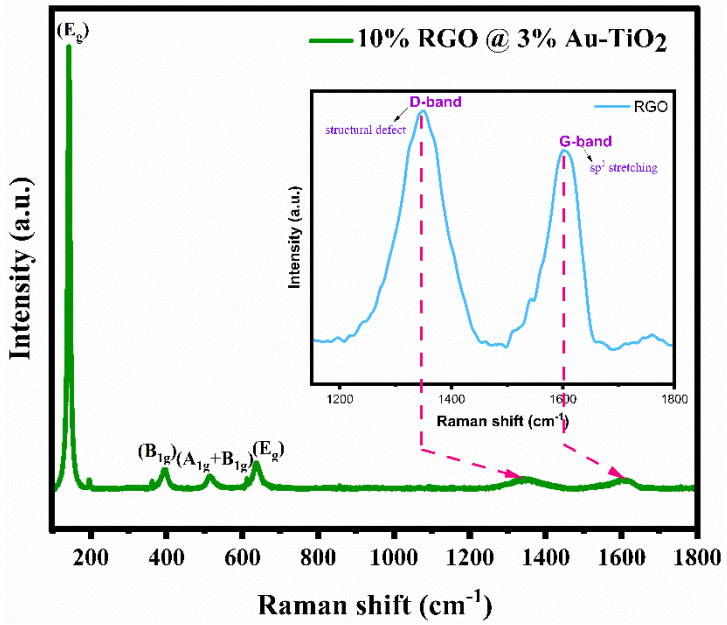

Fig 3.9: Raman of rGO and 10% rGO @ 3%AuTiO_2

UV-Vis DRS & TAUC PLOT

The optical properties of the photocatalysts were tested using UV-Vis DRS. The absorption spectra of TiO_2 show high absorption range around 340 nm, which tells about no absorption in the visible range and is due to intrinsic band-to-band electronic transition from the O 2p valence band to Ti 3d conduction band.

Whereas the absorption spectra of 3% Au-TiO_2 depicts the appearance of absorption band in the visible region, around the range of 565 nm, which is due to the incorporation of Au nanoparticles on TiO_2 surface. The red shift observed after the incorporation of Au nanoparticles is due to LSPR effect, which stands for Localized Surface Plasmon Resonance, it arises from the collective oscillation of conduction electrons under visible light. This metal incorporation also facilitates charge separation. [19, 35, 36, 37]

The absorption spectra of 10% rGO @ 3% Au-TiO_2 depicted further increase in visible light absorption, accompanied by blue shift of plasmonic absorption band 557 nm. This blue shift is due to the interaction between Au nanoparticles, TiO_2 and the conductive rGO sheets. Formation of interfacial bonds due to interaction of Ti and C-O of rGO, also the conductive nature of rGO, adds in to modify the Au nanoparticle dielectric environment, which causes enhanced light absorption in visible region, moreover it also suppresses electron-hole recombination. [19, 38]

The calculated band gaps for TiO_2, 3% Au-TiO_2 and 10% rGO @ 3%Au-TiO_2 are, 3.3, 2.9, and 2.7 eV respectively. The gradual decease in the band gap is observed upon, first by the addition of Au and later rGO. The reduction in band gap due to Au incorporation is due to prior discussed LSPR effect and the incorporation of rGO reduces the band gap as it is very conductive and facilitates charge transfer across the heterojunctions. [19, 37]

The below graphs *Fig 3.10* show the results of UV-DRS and Tauc plot:

SPR & Tauc Plot:

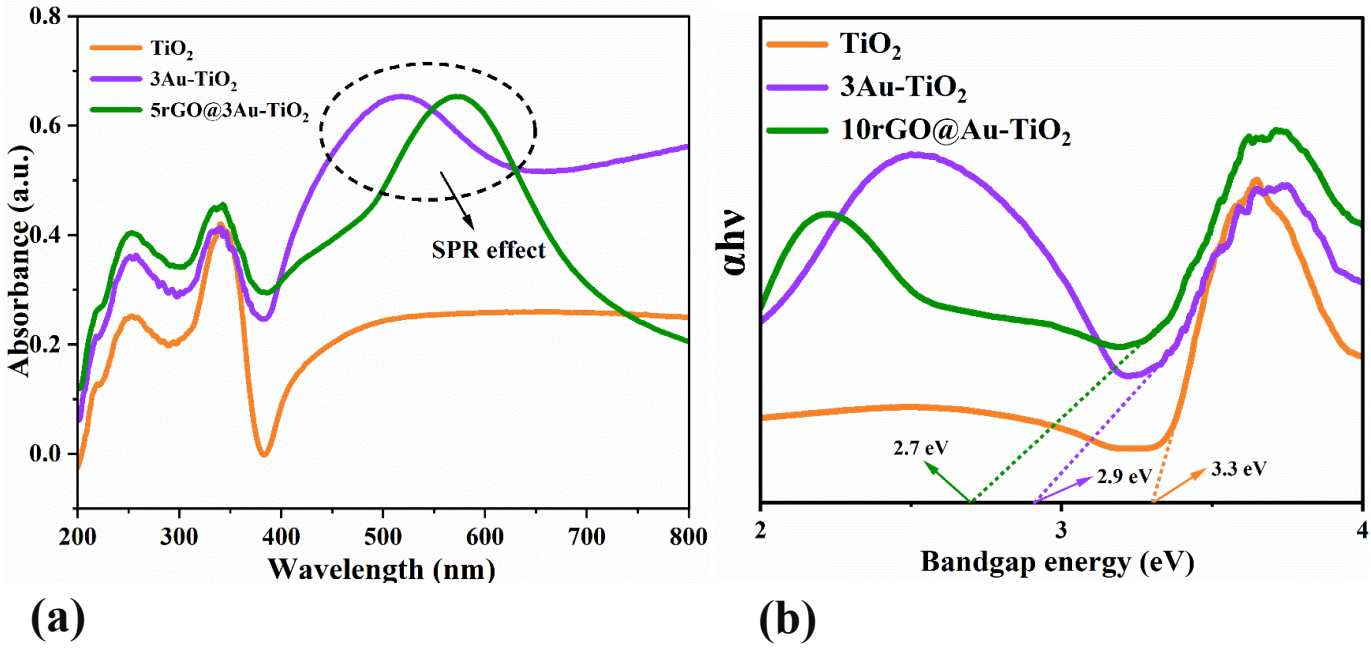

*Fig 3.10: **(a)** SPR effect as shown in the graph is pronoucced in case of 3%Au-TiO_2 and 10%rGO 3%Au-TiO_2 as compared to TiO_2 **(b)** Band gap energies as calculated by UV-DRS Tauc plot of TiO_2 , 3%AuTiO_2 and 10%rGO 3%Au-TiO_2*

XPS

X-ray photoelectron spectroscopy (XPS) was employed to investigate the surface elemental composition and chemical states of the synthesized Au-TiO_2/rGO nanocomposite. The high-resolution Ti 2p spectrum exhibits two characteristic peaks at 458.17 and 463.85 eV, corresponding to Ti $2p_{3/2}$ and Ti $2p_{1/2}$, respectively, with a spin–orbit separation of 5.68 eV. This separation and the corresponding binding energies are characteristic of Ti^{4+} in TiO_2, confirming the presence of the TiO_2 phase in the composite. The O 1s spectrum can be resolved into a dominant component at 529.31 eV, assigned to lattice Ti-O bonds, and a higher-binding-energy component at 531.14 eV associated predominantly with surface hydroxyl/chemisorbed oxygen species. The presence of surface -OH group is particularly relevant to photocatalysis because surface hydroxyl species can participate in the formation of reactive oxygen species during irradiation.

The C 1s spectrum further provides evidence for the carbonaceous component of the nanocomposite. The dominant peak at 284.23 eV is attributed to sp^2 C-C/C=C bonding, while the components at 285.84 and 288.28 eV correspond to oxygenated carbon species such as C-

O and O-C=O, respectively. Such C-O containing surface functionalities are consistent with the presence of oxygen-containing groups associated with the rGO component. The Au 4f spectrum displays the characteristic spin-orbit doublet with a separation of approximately 3.7 eV, supporting the presence of Au species on the TiO_2 surface; however, the unusually low measured binding energy of the Au $4f_{7/2}$ component (82.71 eV) should be interpreted after confirming the energy-scale calibration against an appropriate reference. Overall, the XPS results confirm the co-existence of Ti^{4+}/TiO_2, lattice and surface oxygen species, carbon-containing functionalities and Au species, thereby supporting the successful formation of the Au-TiO_2/rGO composite used in the photocatalytic experiments.

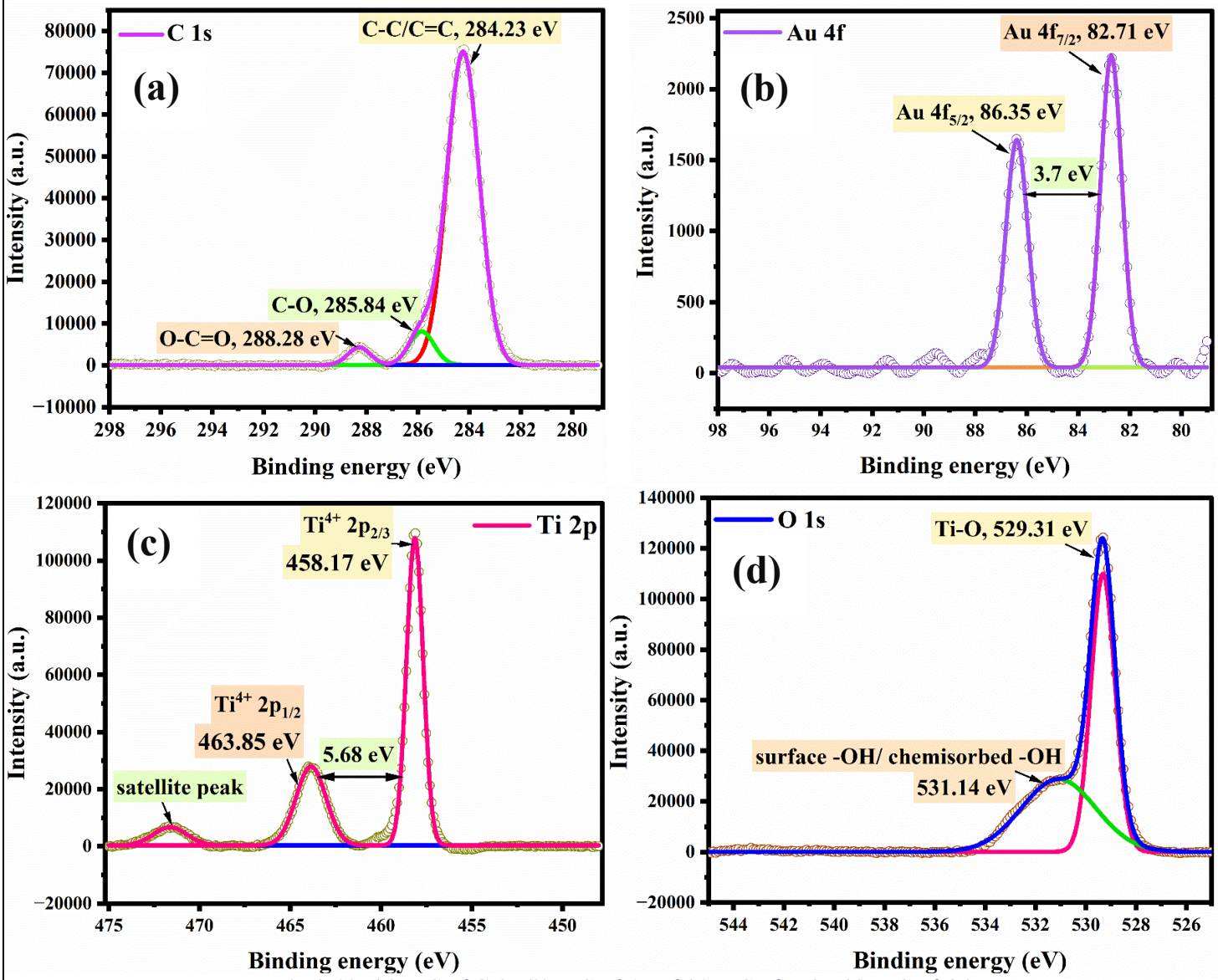

*Fig 3.11: **(a)**XPS of C 1s **(b)**XPS of Au 4f **(c)**XPS of Ti 2p **(d)**XPS of O1s*

3.4 PHOTOCATALYTIC H_2 PRODUCTION

In the experimental setups to produce green hydrogen, successful biomass waste derived cellulose was synthesized which yielded less hydrogen than commercial micro-crystalline cellulose. Due to this reason, the final experimental setups had micro-crystalline cellulose as the sacrificial agent, ethanol as co-substrate & hole scavenger. For the catalysts, various setups, initially to choose the metal, Ag and Au were tested, out of which Au outperformed. So, attempt to make composites containing 1, 3 and 5 wt.% of Au over TiO_2 were tested to produce hydrogen from cellulose in the presence of sunlight, and the setup with 3% Au-TiO_2 gave the maximum hydrogen.

1% Au-TiO_2 was inefficient due to the lower ability to reduce electron-hole recombination as well as LSPR effect; whereas 5% Au-TiO_2 gave poor results than the 3 wt.% due to possibility of excess Au nano-particles blocking the active site of TiO_2, hindering the hydrogen production efficiency.

Furthermore, the selected most-efficient nano-composite was coated with 5, 10 and 12 wt.% of highly conductive material-rGO. Upon the timed study of the hydrogen production of the above prepared catalysts in the sunlight, for 5 h, with intensity in range of 900-1300 W/m^2 during June 2026 at Patiala, Punjab, it was observed that 10 wt.% rGO worked best and produced highest of 296.12 mmol hydrogen.

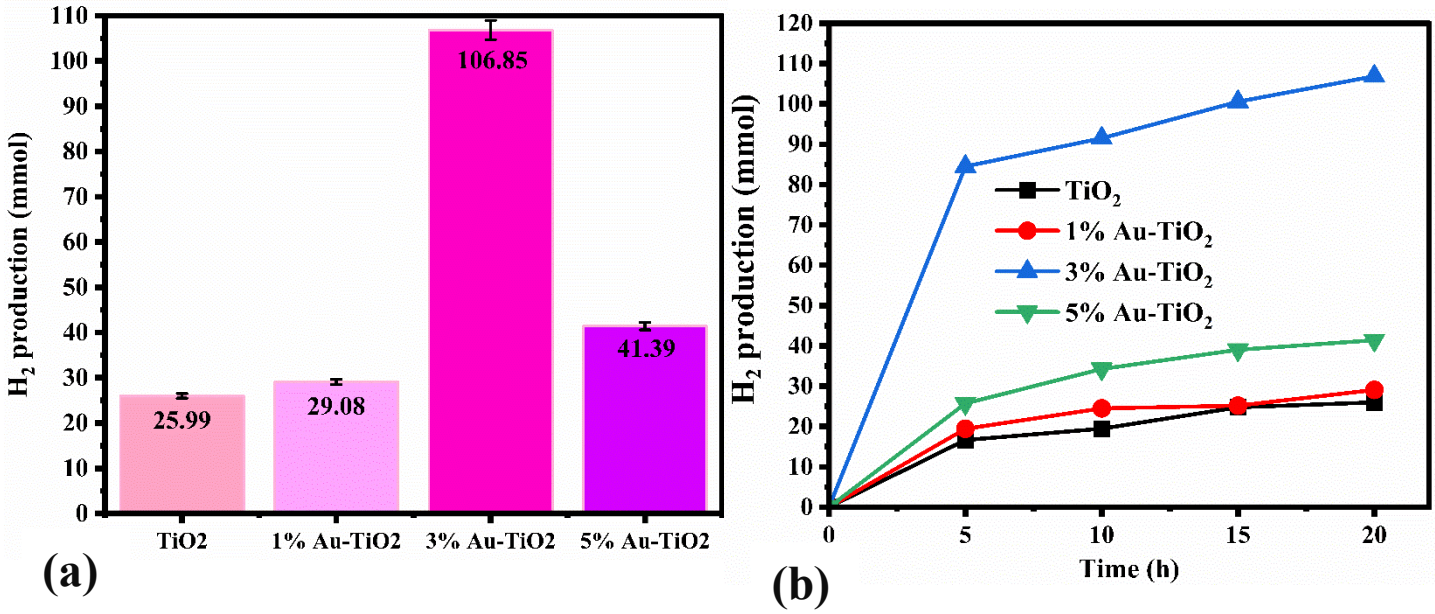

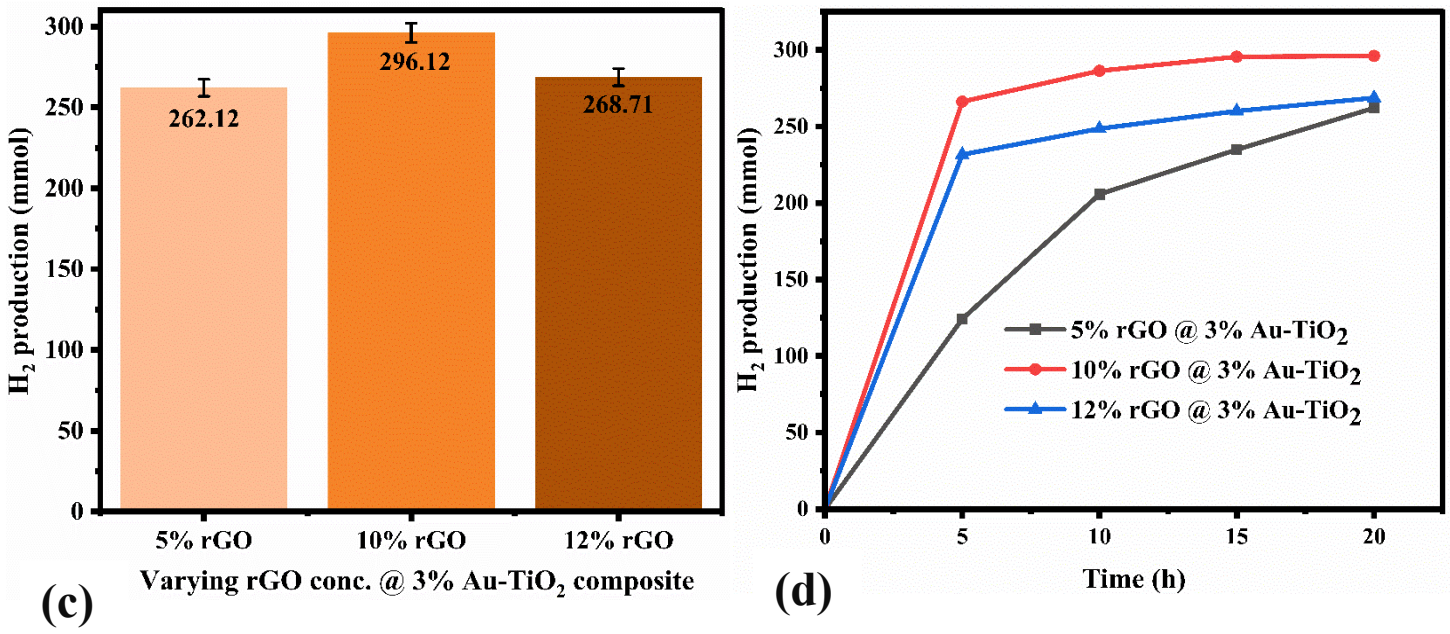

Fig 3.12: *(a) Comparative studies for H_2 production among various wt. % of Au and bare TiO_2*

(b) Kinetic studies of composites of Au-TiO_2, showing most efficient catalyst as 3% Au-TiO_2

(c) Comparative studies for H_2 production among various wt. % of rGO

(d) Kinetic studies of composites of rGO-3%Au-TiO_2, showing most efficient catalyst as 10%rGO 3% Au-TiO_2

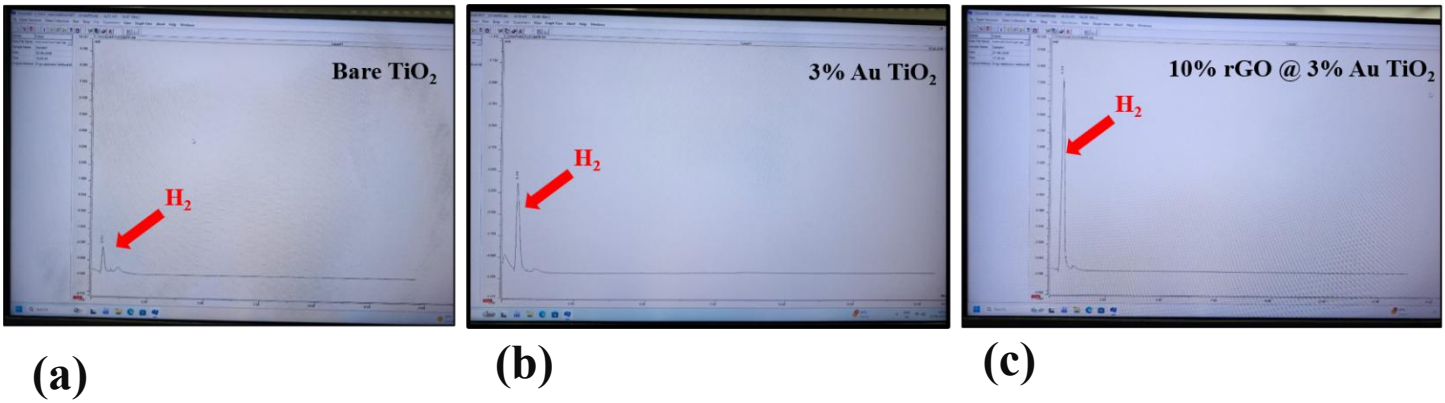

Fig 3.13: *(a) Gas chromatograph of bare TiO_2*

(b) Gas chromatograph of 3% Au-TiO_2

(c) Gas chromatograph of 10% rGO @ 3% Au- TiO_2

3.5 CALCULATION OF H_2 PRODUCTION

Standard hydrogen gas concentration (N_{STD}) = 505 ppm

According to Avogadro's Law: $N_1:V_1 = N_2:V_2$

The relation between standard and sample gas can be expressed as:

$\frac{N_{STD}}{H_{STD}} = \frac{N_{Sample}}{H_{Sample}}$ (where, H stands for peak height of hydrogen in the gas chromatograph)

Rearranging,

$N_{sample} = \frac{N_{STD} \times H_{Sample}}{H_{STD}} = Z_{ppm}$

Since 1 ppm = 1 mg/L, therefore:

$Z_{ppm} = Z_{\frac{mg}{L}} \implies \frac{Z}{1000} = Z_{\frac{g}{L}}$ of H_2

Let:

K= 0.00Z g of H_2

The number of moles of hydrogen:

$$Moles\ (Y) = \frac{Given\ mass}{Molecular\ weight\ of H_2} = \frac{K}{2} = Y\ mol$$

To calculate the volume of space for H_2 used for reaction setup:

Height of headspace in which hydrogen is present = Volume in which H2 is present

The volume of headspace = 32.03 mL

Now, using the definition of molarity:

$$Molarity = \frac{No.of\ moles\ of\ solute}{Vol.of\ solution\ in\ Liters}$$

If Y moles of H_2 are present in the solution volume, then:

1000 ml (1L) → Y mol of H_2

1 ml of solution contains $\frac{Y}{1000}$ moles of H_2

Then, 32.03 ml of solution contains = $\frac{Y\ X\ 32}{1000} = Z\ moles$ of H_2

For example:

Peak height of (H_{std}) standard H_2 = 505 µV

Peak height of sample $H_{Au\text{-}TiO2Nps}$ = 5074 µV

Now, according to formula above $N_{sample} = \frac{505\ X\ 5074}{331}$ = 7,741.2 mg/L or ppm

For no. of moles = 7.741/2 = 3.873 moles, in 1000 ml of solution.

So, 32.03 ml contains, $\frac{3.873\ X\ 32.03}{1000}$ = 0.124 moles of H_2 is present.

Chapter 4 CONCLUSION

This thesis work explored a sustainable route for hydrogen production by bringing together two renewable resources: waste biomass which is sawdust, as the feedstock and sunlight as the clean energy source. The research began with the extraction of cellulose from locally available sawdust through hydrothermal valorisation and alkaline treatment. FTIR analysis showed a reduction in the characteristic contributions of lignin and hemicellulose while retaining the characteristic cellulose features, supporting the successful transformation of the lignocellulosic starting material. Although the extracted cellulose showed lower hydrogen production than commercial microcrystalline cellulose, the results demonstrate the possibility of utilizing an inexpensive waste material as a starting point for photocatalytic hydrogen production.

Along with biomass utilization, the work focused on improving the photocatalytic performance of TiO_2. Different Au loadings, 1, 3 & 5 wt. % were investigated, among which 3 wt.% Au-TiO_2 showed the highest photocatalytic activity. Lower Au loading was not sufficient to provide the desired enhancement, whereas excessive Au loading likely reduced the availability of active sites. The optimized 3% Au-TiO_2 was therefore further modified with rGO, and among the compositions investigated for 5, 10 % 12 wt. %, 10% rGO-3% Au-TiO_2 showed the best hydrogen evolution performance under solar irradiation.

The characterisation results supported the successful development of the photocatalytic system. XRD confirmed that the anatase crystalline structure of TiO_2 was retained after modification, while FE-SEM and EDS supported the incorporation of Au and rGO in the prepared composites. Raman spectroscopy further confirmed the presence of rGO through its characteristic D and G bands. Most importantly, modification produced a clear improvement in the optical response of TiO_2. The estimated band-gap energy decreased from 3.03 eV for TiO_2 to 2.95 eV for 3% Au-TiO_2 and further to 2.86 eV for 10% rGO-3% Au-TiO_2. The appearance of plasmonic absorption in the visible region after Au incorporation, together with the enhanced absorption after rGO modification, indicates better utilization of the solar spectrum. XPS analysis confirmed the successful formation of the Au-TiO_2/rGO nanocomposite. The characteristic Ti 2p and O 1s peaks confirmed Ti^{4+} and Ti-O bonding in TiO_2, while the C 1s spectrum indicated the presence of carbonaceous and oxygen-containing functionalities associated with rGO. The Au 4f doublet further confirmed the incorporation of Au species on the TiO_2 surface. These results collectively support the successful integration of

TiO_2, Au and rGO, providing the desired surface chemical characteristics for enhanced photocatalytic activity.

Overall, the work demonstrates that the photocatalytic activity of TiO_2 can be improved through a combination of plasmonic Au loading and rGO-assisted charge transfer, while cellulose can serve as an organic substrate for solar-driven hydrogen evolution. The highest hydrogen production was obtained with the optimized 10% rGO @ 3% Au-TiO_2 photocatalyst, showing the advantage of the ternary system over bare TiO_2 and Au-TiO_2. More importantly, the work provides a small but meaningful insight towards connecting waste valorisation with renewable hydrogen production.

REFRENCES

[1] P, Friedlingstein; et al., Global Carbon Budget 2023. *Earth Syst Sci Data*, **2023**, *15*, 5301-5369. doi: 10.5194/essd-15-5301-2023.

[2] S, Griffiths; B, K, Sovacool; J, Kim; M, Bazilian; J, M, Uratani. Industrial decarbonization via hydrogen: A critical and systematic review of developments, socio-technical systems and policy options. *Energy Res Soc Sci*. **2021**, *80*, 102208. doi: 10.1016/j.erss.2021.102208.

[3] M, Höök; X, Tang. Depletion of fossil fuels and anthropogenic climate change—A review. *Energy Policy*, **2013**, *52*, 797-809. doi: 10.1016/j.enpol.2012.10.046.

[4] P, M, Forster; et al. Indicators of Global Climate Change 2024: annual update of key indicators of the state of the climate system and human influence. *Earth Syst Sci Data*, **2015**, *17*, 2641-2680. doi: 10.5194/essd-17-2641-2025.

[5] I, Dincer. Renewable energy and sustainable development: a crucial review. *Renew Sustain Energy Rev*, **2000**, *4*, 157-175. doi: 10.1016/S1364-0321(99)00011-8.

[6] E, Rivard; M, Trudeau; K, Zaghib. Hydrogen Storage for Mobility: A Review. *Materials*, **2019**, *12*, 1973. doi: 10.3390/ma12121973.

[7] L, Schlapbach; A, Züttel; Hydrogen-storage materials for mobile applications. *Nature*, **2001**, *414*, 353-8. doi: 10.1038/35104634.

[8] I, Dincer; C, Acar. Review and evaluation of hydrogen production methods for better sustainability. *Int J Hydrogen Energy*. **2015**, *40*, 11094-11111. doi: 10.1016/j.ijhydene.2014.12.035.

[9] A, V, Bridgwater. Review of fast pyrolysis of biomass and product upgrading. *Biomass Bioenergy*, **2012**, *38*, 68-94. doi: 10.1016/j.biombioe.2011.01.048.

[10] Y, Yao; X, Gao; Z, Li; X, Meng. Photocatalytic Reforming for Hydrogen Evolution: A Review. *Catalysts*, **2020**, *10*, 335. doi: 10.3390/catal10030335.

[11] M, Noussan; P, P, Raimondi; R, Scita; M, Hafner. The Role of Green and Blue Hydrogen in the Energy Transition-A Technological and Geopolitical Perspective. *Sustainability*, **2021**, *13*, 298. doi: 10.3390/su13010298.

[12] D, I, Kondarides; V, M, Daskalaki; A, Patsoura; X, E, Verykios; Hydrogen production by photo-induced reforming of biomass components and derivatives at ambient conditions. *Catal Lett*, **2008**, *122*, 26-32. doi: 10.1007/s10562-007-9330-3.

[13] X, Fu; et al. Photocatalytic reforming of biomass: A systematic study of hydrogen evolution from glucose solution. *Int J Hydrogen Energy*, **2008**, *33*, 6484-6491. doi: 10.1016/j.ijhydene.2008.07.068.

[14] K, Nakata; A, Fujishima. TiO_2 photocatalysis: Design and applications. *J Photochem Photobiol C,* **2012**, *13*, 169-189. doi: 10.1016/j.jphotochemrev.2012.06.001.

[15] M, R, Hoffmann; S, T, Martin; W, Choi; D, W, Bahnemann. Environmental applications of semiconductor photocatalysis. *Chem Rev*, **2002**, *1995*, 69-96. doi: 10.1021/cr00033a004.

[16] A, Mills; S, Le Hunte; An overview of semiconductor photocatalysis. *J Photochem Photobiol A*, **1997**, *108*, 1-35. doi: 10.1016/S1010-6030(97)00118-4.

[17] W-T, Chen; A, Chan; D, Sun-Waterhouse; J, Llorca; H, Idriss; G, I, N, Waterhouse; Performance comparison of Ni/TiO_2 and Au/TiO_2 photocatalysts for H_2 production in different alcohol-water mixtures. *J Catal*, **2018**, *367*, 27-42. doi: 10.1016/j.jcat.2018.08.015.

[18] A, Tanaka; S, Sakaguchi; K, Hashimoto; H, Kominami. Preparation of Au/TiO_2 with metal cocatalysts exhibiting strong surface plasmon resonance effective for photoinduced hydrogen formation under irradiation of visible light. *ACS Catal*, **2013**, *3*, 79-85. doi: 10.1021/cs3006499.

[19] S, Kochar; B, Pal. Photocatalytic hydrogen production from dextrose by GO modified Ag-TiO2 nanorods under UV/solar irradiation. *Biomass Bioenergy*, **2026**, *204*, 108441. doi: 10.1016/j.jhazmat.2012.02.063.

[20] H, M, El-Bery; Y, Matsushita; A, Abdel-moneim. Fabrication of efficient TiO_2-RGO heterojunction composites for hydrogen generation *via* water-splitting: Comparison between RGO, Au and Pt reduction sites. *Appl Surf Sci*, **2017**, *423*, 185-196. doi: 10.1016/j.apsusc.2017.06.140.

[21] Y, Liu; Hydrothermal synthesis of TiO_2-RGO composites and their improved photocatalytic activity in visible light. *RSC Adv*. **2015**, *68*, 36040-36045. doi: 10.1021/jz100728z.

[22] A, Caravaca; W, Jones; C, Hardacre; M, Bowker. H_2 production by the photocatalytic reforming of cellulose and raw biomass using Ni, Pd, Pt and Au on titania. *Proc Math Phys Eng Sci.* **2016**, *472*, 20160054. doi: 10.1098/rspa.2016.0054.

[23] G, Zhang; et al. Simultaneous cellulose conversion and hydrogen production assisted by cellulose decomposition under UV-light photocatalysis. *Chem Commun*, **2015**, *52*, 1673-1676. doi: 10.1039/C5CC09075J.

[24] A, Fujishima; K, Honda. Electrochemical photolysis of water at a semiconductor electrode. *Nature*, **1972**, *238*, 37-38. doi: 10.1038/238037a0.

[25] A, Patsoura; D, I, Kondarides; X, E, Verykios. Enhancement of photoinduced hydrogen production from irradiated Pt/TiO2 suspensions with simultaneous degradation of azo-dyes. *Appl Catal B*, **2006**, *64*, 171-179. doi: 10.1016/j.apcatb.2005.11.015.

[26] P, Gomathisankar; D, Yamamoto; H, Katsumata; T, Suzuki; S, Kaneco; Photocatalytic hydrogen production with aid of simultaneous metal deposition using titanium dioxide from aqueous glucose solution. *Int J Hydrogen Energy*, **2013**, *38*, 5517-5524. doi: 10.1016/j.ijhydene.2013.03.014.

[27] A, V, Puga; Photocatalytic production of hydrogen from biomass-derived feedstocks. *Coord Chem Rev*, **2016**, *315*, 1-66. doi: 10.1016/j.ccr.2015.12.009.

[28] S, K, Lakhera; A, Rajan; R, T, P; N, Bernaurdshaw; A review on particulate photocatalytic hydrogen production system: Progress made in achieving high energy conversion efficiency and key challenges ahead. *Renew. Sustain. Energy Rev*. **2021**, *152*, 11694. doi: 10.1246/cl.1981.81.

[29] D, W, Wakerley; M, F, Kuehnel; K, L, Orchard; K, H, Ly; T, E, Rosser; E, Reisner; Solar-driven reforming of lignocellulose to H_2 with a CdS/CdOx photocatalyst. *Nat Energy*, **2017**, *2*, 17021. doi: 10.1038/nenergy.2017.21.

[30] H, Kasap; D, Achilleos; A, Huang; E, Reisner. Photoreforming of lignocellulose into H_2 using nanoengineered carbon nitride under benign conditions. *J Am Chem Soc*, **2018**, *140*, 11604-11607. doi: 10.1021/jacs.8b07853.

[31] S, Y, A, Salgado; R, M, R, Zamora; R, Zanella; J, Peral; S, Malato; M, I, Maldonado. Photocatalytic hydrogen production in a solar pilot plant using a Au/TiO_2 photocatalyst. *Int J Hydrogen Energy*, **2016**, *41*, 11933-11940. doi: 10.1016/j.ijhydene.2016.05.039.

[32] C, Chang; et al. Using cellulose polymorphs for enhanced hydrogen production from photocatalytic reforming. *Sustain Energy Fuels*, **2019**, *3*, 1971-1975. doi: 10.1039/C9SE00377K.

[33] M, Mergbi; et al. Valorization of lignocellulosic biomass into sustainable materials for adsorption and photocatalytic applications in water and air remediation. *Environ. Sci. Pollut. Res.* **2023**, *30*, 74544-74574. doi: 10.1039/C9GC01728C.

[34] S, Rani; S, Singh; B, Pal. Superior photocatalytic activity of g-C3N4@Cu-TiO2 core shell structure for hydrogen production from H2O splitting and C2H5OH dehydrogenation under solar light. *Renew. Energy*, **2025**, *253*, 123634. https://doi.org/10.1016/j.renene.2025.123634

[35] P. Soni; B, Pal; R, K, Das. Enhanced photocatalytic urea oxidation under neutral medium by reduced graphene oxide coated TiO_2 nanoparticles. *Catal. Commun*. **2023**, *179*, 106690. https://doi.org/10.1016/j.catcom.2023.106690

[36] D, Kaur; K, Singh; W, T, Reynolds Jr; B, Pal. Graphene oxide-coated Ag-TiO2 hybrid nanocomposites for superior photocatalytic activity. *Environ. Sci. Pollut. Res*. **2023**, *30*, 97660-97672. https://doi.org/10.1007/s11356-023-29301-2

[37] R, A, Rather; S, Singh; B, Pal. Core-shell morphology of Au-TiO_2 @ graphene oxide nanocomposite exhibiting enhanced hydrogen production from water. *J. Ind. Eng. Chem*. **2016**, *37*, 288-294. http://dx.doi.org/10.1016/j.jiec.2016.03.039

[38] E, Pinto; et al. Cellulose processing from biomass and its derivation into carboxymethylcellulose: A review. *Sci. Afr*. **2022**, *15*, 1078. https://doi.org/10.1016/j.sciaf.2021.e01078

[39] R, S, Abolore; S, Jaiswal; A, K, Jaiswal. Green and sustainable pretreatment methods for cellulose extraction from lignocellulosic biomass and its applications: A review. *Carbohydr. Polym. Technol. Appl.* **2024**, *7*, 100396. https://doi.org/10.1016/j.carpta.2023.100396

[40] A-C, Macarez; et al. From olive stones waste to valuable resource: Exploring various techniques for cellulose extraction. *J. Environ. Chem. Eng*. **2025**, *13*, 118204. https://doi.org/10.1016/j.jece.2025.118204

[41] M, B, da Silva; et al. Evaluating Sodium Hydroxide and Hydrogen Peroxide as Chemical Treatment for Cellulose Extraction from *Clitoria fairchildiana* Pruning Residues. *Reactions*, **2025**, *6*, 60. https://doi.org/10.3390/reactions6040060

[42] H, A, Rasheed; et al. Isolation, characterization and response surface method optimization of cellulose from hybridized agricultural wastes, *Sci. Rep*. **2024**, *14*, 14310. https://doi.org/10.1038/s41598-024-65229-4

MT

ORIGINALITY REPORT

11%	8%	7%	%
SIMILARITY INDEX	INTERNET SOURCES	PUBLICATIONS	STUDENT PAPERS

PRIMARY SOURCES

1	Shikha Rani, Satnam Singh, Bonamali Pal. "Core-shell structure of reduced graphene oxide@Ag–TiO2 for photocatalytic H2O splitting and CH3OH dehydrogenation under UV light irradiation", International Journal of Hydrogen Energy, 2023 Publication	4%
2	tudr.thapar.edu Internet Source	4%
3	mdpi-res.com Internet Source	<1%
4	www.eprint.iitd.ac.in Internet Source	<1%
5	Dipankar Gogoi, Ananta Sasmal, T.D. Das. "Tailoring surface defects and interface states in nanocrystalline organometallic perovskites for high-performance solar cells", Journal of Alloys and Compounds, 2026 Publication	<1%
6	www.hindawi.com Internet Source	<1%
7	iopscience.iop.org Internet Source	<1%
8	www.frontiersin.org Internet Source	<1%
9	Liao, Chi-Hung, Chao-Wei Huang, and Jeffrey C. S. Wu. "Hydrogen Production from Semiconductor-based Photocatalysis via Water Splitting", Catalysts, 2012. Publication	<1%
10	M. Klavins, L. Eglite, J. Serzane. "Methods for Analysis of Aquatic Humic Substances", Critical Reviews in Analytical Chemistry, 1999 Publication	<1%
11	oro.open.ac.uk Internet Source	<1%
12	doczz.net Internet Source	<1%

13	vdoc.pub Internet Source	<1%
14	idr-sdlib.iitbhu.ac.in Internet Source	<1%
15	tudr.thapar.edu:8080 Internet Source	<1%
16	www.smolecule.com Internet Source	<1%
17	www.yanglonggroup.com Internet Source	<1%
18	Sleipness, E.P.. "Contribution of the suprachiasmatic nucleus to day:night variation in cocaine-seeking behavior", Physiology & Behavior, 20070815 Publication	<1%
19	etheses.whiterose.ac.uk Internet Source	<1%
20	nadre.ethernet.edu.et Internet Source	<1%
21	Ali Tahir, Asif, Habib Ullah, Pitchaimuthu Sudhagar, Mohd Asri Mat Teridi, Anitha Devadoss, and Senthilarasu Sundaram. "The Application of Graphene and Its Derivatives to Energy Conversion, Storage, and Environmental and Biosensing Devices", The Chemical Record, 2016. Publication	<1%
22	Kong, Ziyin. "Design, Synthesis and Functionalization of Geminal and Vicinal Organometallic Compounds", Boston College, 2024 Publication	<1%
23	guan.nankai.edu.cn Internet Source	<1%
24	pubs.rsc.org Internet Source	<1%
25	static.akcongress.com Internet Source	<1%

Exclude quotes	Off	Exclude matches	Off
Exclude bibliography	Off		

Pragnaya Raina